DEFENSE DOCUMENTATION CENTER

FOR

SCIENTIFIC AND TECHNICAL INFORMATION

CAMERON STATION, ALEXANDRIA, VIRGINIA

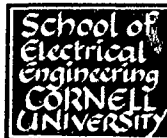**School of Electrical Engineering CORNELL UNIVERSITY**

CORNELL UNIVERSITY

SCHOOL OF ELECTRICAL ENGINEERING

RESEARCH REPORT EE 539

An Investigation of the Laminarity of Flow
in a Magnetically Confined Electron Beam

DDC

JUN 21 1963

15 September 1962
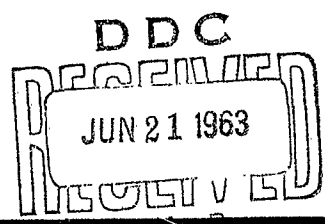
D. D. Hallock

School of Electrical Engineering
CORNELL UNIVERSITY
Ithaca, New York

RESEARCH REPORT EE 539

AN INVESTIGATION OF THE LAMINARITY OF FLOW
IN A MAGNETICALLY CONFINED ELECTRON BEAM

D. D. Hallock

LINEAR BEAM MICROWAVE TUBES

Technical Report No. 19   15 September 1962

ACKNOWLEDGMENTS

CONTENTS

ABSTRACT

A study of the electron flow in a Brillouin beam was made, which yielded information that provided an insight into the electron behavior in a medium-power Brillouin beam. It was shown that the beam can display a high degree of laminarity at a beam voltage of 5000 v.

The trajectory equation of the outer edge electron in the laminar model of the beam was linearized and shown to give results in good agreement with the experimental observations, when the focusing field was less than twice the Brillouin field. It was also shown that the beam can be focused at the calculated Brillouin field within the limits of experimental error. The differences between the theoretical predictions and the experimental observations, which arose from limitations either of the experimental apparatus or the theory, are discussed. The effects of thermal velocities are considered particularly at low beam voltages.

I. INTRODUCTION

Since the advent of the linear beam microwave tube in World War II, the motion of electrons in cylindrical electron beams has been the subject of several theoretical and experimental studies, because a knowledge of the electron motion in the beam is important in formulating a r-f theory for the modulated beam. The simplest theories describing the velocity-modulated beam assume a beam that is laminar, free from any d-c axial variation, and with constant charge density in the radial and angular directions. While this is a highly idealized model of the beam, it is very simple and has led to theoretical predictions which have been subsequently verified experimentally. [1]

The purpose of this study was to determine the degree of laminarity of the beam from an STL-100 electron gun.* This would serve as a basis for interpreting future r-f measurements made with this beam and provide a basic insight into the electron behavior in a medium-power beam from a shielded Pierce gun. Although much work has been done on electron beams, most of it has been under at least one of the following restrictive conditions: (1) focus fields much higher than the calculated Brillouin[2] field, (2) low beam voltage, (3) low current density. Very few detailed studies have been made of the electron flow in the medium- and high-power beams, which are coming into more general use in present-day linear beam tubes. Some work in this direction was done by Gilmour,[3] who reported that the STL-100 beam seemed to show a high degree of laminarity. He discovered certain anomalies, however, which he could

---

*This was one of five donated to the School of Electrical Engineering by the Sperry Gyroscope Company.

standing of the problem was obtained, however.   A discussion of the perturbation experiment, and an analysis of the results are given in Appendix B.

II. THEORETICAL ANALYSIS

The theory of the electron motion in a laminar electron beam is presented as a basis for discussion of the experimental observations. In general the approach used follows the one used by Wang.[4]

A. DERIVATION OF TRAJECTORY EQUATION

In the laminar model the electron beam is described as an infinite number of concentric, cylindrical shells. An electron is injected into a given shell at the plane of origin (the cathode) and remains in that shell until the beam is terminated. Under these conditions any electron trajectory may be described in cylindrical co-ordinates by

$$r_i(z) = \mu \, r(z) \quad , \tag{1}$$

where r is the radius of the outer-edge electron shell as shown in Figure 1, and r_i is the radius of any internal electron shell. Since for laminar flow, μ is a constant, only the trajectory of the outer edge electron shell need be determined to describe the electron motion in the beam completely.

The Hamiltonian function in cylindrical co-ordinates is;

$$H = \frac{1}{2} m \, (\dot{r}^2 + \dot{z}^2 + r^2 \dot{\theta}^2) - e\phi = 0 \quad , \tag{2}$$

which expresses the fact that the system is conservative. The equation of motion for the electron beam can be obtained by using the three Hamiltonian equations:

$$\frac{dP_r}{dt} = -\frac{\partial H}{\partial r} \quad , \qquad \frac{dP_z}{dt} = -\frac{\partial H}{\partial z} \quad , \qquad \frac{dP_\theta}{dt} = -\frac{\partial H}{\partial \theta} \quad , \tag{3}$$

-4-

FLUX LINE THROUGH EDGE OF CATHODE

B

ANODE EXIT. MAGNETIC FIELD BROUGHT IN AT Z=0

Z=0
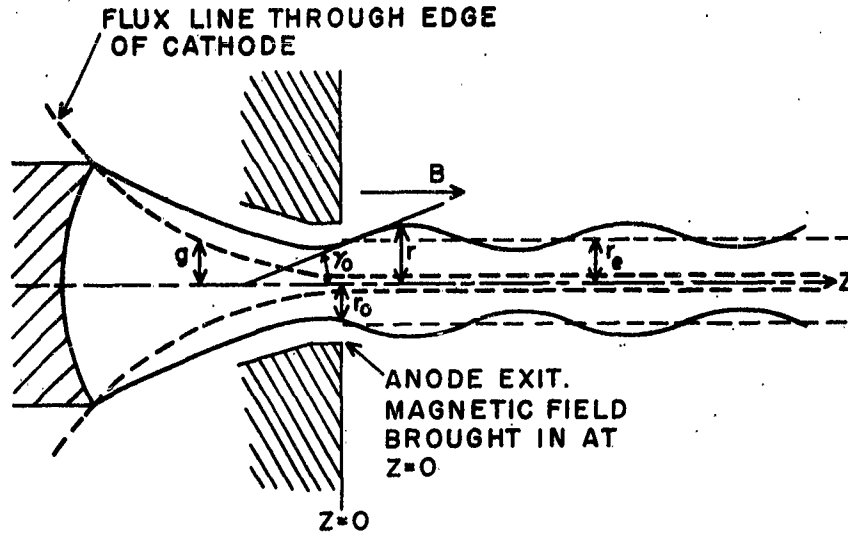
Figure 1. Diagram of Electron Beam Showing Some of Parameters Used in Deriving Laminar Theory.

where P_r, P_z, and P_θ are the generalized moments.

Since B, the magnetic field, is represented by a solenoidal vector, it can be expressed as the curl of a magnetic vector potential, A. Because of the axial symmetry of the magnetic field, only the A_θ component of the vector potential is required. The magnetic field components may be written as

$$B_z = \frac{1}{r} \frac{\partial_r A_\theta}{\partial r} \quad , \quad B_r = - \frac{\partial A_\theta}{\partial z} \quad . \tag{4}$$

The velocities may be eliminated from H by using

$$P_r = m\dot{r} \quad , \tag{5a}$$

$$P_z = m\dot{z} \quad , \tag{5b}$$

$$P_\theta = m r^2 \dot{\theta} - e r A_\theta \quad . \tag{5c}$$

The Hamiltonian then becomes

$$H = \frac{1}{2m} \left[P_r^2 + P_z^2 + \left(\frac{P_\theta}{r} + e A_\theta \right)^2 \right] - e\phi = 0 \quad . \tag{6}$$

-5-

The operations indicated in Equation (3) are performed on this equation to obtain the following equations of motion:

$$\ddot{r} = r\,\dot{\theta}^2 - \eta r\,\dot{\theta}\,B_z + \eta\frac{\partial\theta}{\partial r} \quad , \qquad (7a)$$

$$\ddot{z} = \eta r\,\dot{\theta}\,B_r + \frac{n\partial\phi}{\partial z} \quad , \qquad (7b)$$

$$\frac{d}{dt}\,(r^2\,\dot{\theta} - \eta r\,A_\theta) = 0 \quad , \qquad (7c)$$

where η is the electron charge-to-mass ratio, and where it has been assumed that the potential ϕ is axially symmetric ($\partial\phi/\partial\theta = 0$). Equation (7c) may be integrated directly to yield

$$r^2\,\dot{\theta} = \eta\,(r\,A_\theta - r_c\,A_{\theta_c}) \quad , \qquad (8)$$

where A_{θ_c} is a measure of flux through the cathode. For the case studied, the magnetic field was independent of r and z in the drift region; therefore

$$A_\theta = \frac{r}{2}\,B_z \qquad (9)$$

from Equation (4), and Equation (8) becomes

$$\dot{\theta} = \omega_L\,\left(1 - \frac{g^2}{r^2}\right) \quad , \qquad (10)$$

where $\omega_L = \eta B/2$, the Larmor angular frequency, and g is the radius of the flux line through the edge of the cathode at the plane where θ is to be determined as shown in Figure 1.

The term $\partial\phi/\partial r$ of Equation (7a), which is the radial component of the electric field in the presence of space charge, must still be determined. From Poisson's equation,

$$\mathrm{div}\ E = \frac{1}{r}\,\frac{d(r\,E_r)}{dr} = \frac{\rho}{\epsilon_0} \quad , \qquad (11)$$

the radial field strength E_r within the beam ($\mu \lesssim 1$) is obtained. This is based on the assumption that the axial field that is due to axial variations in charge density arising from scalloping of the beam can be disregarded. Since $B_r = 0$ for this case, this assumption also means that $\ddot{z}$ will be very small and need not be considered.

Integrating Equation (11) yields

$$E_r = \frac{\rho r}{2 \epsilon_o} \qquad .$$
(12)

The actual space-charge density, ρ, cannot be exactly specified in the beam. A good approximation is obtained by writing

$$\rho = \frac{I_o}{\pi r^2 u} \qquad ,$$
(13)

where I_o is the beam current and u is the z-directed beam velocity; ρ and u should be independent of r when this approximation is used. (From observations on the beam cross section it has been seen that ρ is indeed very nearly independent of r.) For the Brillouin beam (g = 0), Wang[4] has shown that u is independent of the beam radius and has the value,

$$u = \sqrt{2 n (V_b + \phi_s)} \qquad ,$$

where V_b is the potential at the beam edge, and ϕ_s is due to the negative potential depression at the beam center caused by the space charge in the beam. Gilmour[3] has tabulated u as a function of the ratio of beam radius to drift-tube radius for a beam of microperveance one.

Using Equations (10), (12), and (13) in Equation (7a) gives

$$\ddot{r} = - r \left[\omega_L^2 - (\omega_L \frac{g^2}{r^2} - \dot{\theta}_c^2) \right] + \frac{\eta I_o}{2 \pi \epsilon_o r u} \qquad .$$
(14)

By writing $R = r/a$ and $R_g = g/a$, where

$$a = \frac{1}{\omega_L} \sqrt{\frac{\eta I_o}{2\pi \epsilon_o u}} \quad , \tag{15}$$

one finds that Equation (14) becomes

$$\ddot{R} + \omega_L^2 \left[R \left(1 - \frac{R_g^4}{R^4} \right) - \frac{1}{R} \right] = 0 \quad . \tag{16}$$

This equation describes nonlinear oscillations about an equilibrium radius R_e at which $\ddot{R} = 0$. After some manipulation, we get

$$R_e = \left[\frac{1}{2} + \frac{1}{2} \left(1 + 4 R_g^4 \right)^{\frac{1}{2}} \right]^{\frac{1}{2}} \quad . \tag{17}$$

It is seen that for the Brillouin beam (g = 0),

$$R_e = 1 \quad ,$$

or

$$r_e = a \quad .$$

Thus the normalizing term specified in Equation (15) is the equilibrium radius for the Brillouin beam.

B. SCALLOP WAVELENGTH FROM LINEARIZED TRAJECTORY EQUATION

Equation (16) is not very useful for calculations in the form given. For this study, however, only values of the focusing field near that value that produces a Brillouin beam with no radial oscillations are studied. The

-8-

radial deviations from the equilibrium radius should therefore be small,
and the normalized beam radius may be written as

$$R = R_e (1 + \delta) \quad ,$$

where δ is small, such that

$$\frac{1}{1 + \delta} = 1 - \delta \quad ,$$

$$\frac{1}{(1 + \delta)^3} = 1 - 3\delta \quad .$$

Then Equation (17) becomes

$$\ddot{\delta} + \omega_L^2 \, \delta \left[1 + \frac{3 R_g^4}{R_e^4} + \frac{1}{R_e^2} \right] = \left[\frac{R_g^4}{R_e^4} + \frac{1}{R_e^2} - 1 \right] \omega_L^2 \quad .$$

From the definition of R_e given in Equation (17), it is easily shown
that the term on the right-hand side is equal to zero, so that

$$\ddot{\delta} + \omega_L^2 \, \delta \left[1 + \frac{3 R_g^4}{R_e^4} + \frac{1}{R_e^2} \right] = 0 \quad . \tag{18}$$

Some predictions of the beam behavior for a few special cases can
be made on the basis of this equation. The simplest case is that of the
perfect Brillouin beam for which Equation (18) becomes

$$\ddot{\delta} + 2 \omega_L^2 \, \delta = 0 \quad . \tag{19}$$

This equation describes radial oscillations at the scallop frequency
$\omega_s = \sqrt{2} \omega_L$. When ρ is calculated from Equation (13) using the equilibrium
radius as given by Equation (15), then

$$\omega_s = \sqrt{2} \omega_L = \omega_p \quad , \tag{20}$$

where ω_p is the plasma frequency, and $\omega_p = \left(\frac{n}{\epsilon_o}\right)^{\frac{1}{2}}$. It should be noted that Equation (20) has been obtained without the restriction that the beam does not scallop. The amplitude of the beam scallops cannot be very large, however, or the restrictions placed on δ in deriving the linearized Equation (18) will not hold.

The scallop wavelength can be readily obtained from Equation (20):

$$\lambda_s = \frac{2\pi u}{\sqrt{2}\ \omega_L} = \sqrt{2}\ \frac{2\pi u}{\omega_c} = \sqrt{2}\ \lambda_c \ , \tag{21}$$

where λ_c is the cyclotron wavelength, and $\omega_c = \eta B$ is the cyclotron frequency.

The opposite extreme from the case $g = 0$ is when $R_g/R_e = 1$. This is analogous to the case of confined flow in which all the focusing flux threads the cathode, and very high magnetic fields are used. It can readily be shown from Equation (17), however, that the condition $R_g = R_e$ can only be met at $R_e = 0$, which is not a physically realizable case. The problem arises from the term $1/R$ in Equation (16), which represents the space charge of the beam. Because of this term, the equilibrium radius, R_e, of the beam in the drift region must be larger than the radius of the flux line threading the edge of the cathode. This expansion of the beam allows the electron trajectories to encircle more magnetic flux in the drift region than at the cathode, so that the inward-directed Lorentz force can balance the outward-directed space-charge force.

For the case of zero space charge,

$$\omega_s = \omega_c \ ,$$

$$\lambda_s = \lambda_c \ . \tag{22}$$

-10-

When the space charge of the beam is considered, Equation (22) serves as an asymptotic limit to the scallop wavelength as the magnetic field is increased.

For those cases where some flux threads the cathode, the scallop wavelength will be intermediate between λ_c and $\sqrt{2}\,\lambda_c$. The value predicted by the theory must be calculated for the parameters of the system being studied, where

$$\omega_s = \omega_L \left[1 + \frac{3R_g^4}{R_e^4} + \frac{1}{R_e^4} \right]^{\frac{1}{2}} , \qquad (23a)$$

$$\lambda_s = 2\,\lambda_c \left[1 + \frac{3R_g^4}{R_e^4} + \frac{1}{R_e^2} \right]^{\frac{1}{2}} , \qquad (23b)$$

and R_e is given by Equation (17). It should be noted that these equations are still subject to the condition that $\delta \ll 1$ under which the linearized equation was derived.

C. MAGNITUDE OF BEAM SCALLOPS

In a practical tube design, the magnitude of beam scallops is of great importance. This has been determined by previous workers, but not in the form best suited to this study. The values of R_{max} and R_{min} can be obtained by integrating Equation (16). If this equation is multiplied by $2\dot{R}$ it can be integrated directly to yield

$$\dot{R}^2 + \omega_L^2 \left[R^2 + \frac{R_g^4}{R^2} - 2\ln R \right] = C ; \qquad (24)$$

C is a constant that is evaluated from the boundary conditions at the plane of injection into the focusing field. In this study this plane is referred to as the anode exit.

-11-

It has been observed experimentally that the case of zero amplitude scallops can almost be obtained with the beam from the STL-100 electron gun. This suggests that the radial velocity at the anode exit is zero or $\dot{R}_o = 0$. Scalloping does occur, however, when the magnetic field is set either above or below the value for zero amplitude scallops. Since $\dot{R}_o = 0$, this corresponds to the case $R_o \neq R_e$, which is to be expected, since R_e is a function of the magnetic field. The boundary conditions can then be written as

$$R_o = A \, R_e \quad , \tag{25}$$

$$\dot{R}_o = 0 \quad ;$$

then

$$C = \omega_L^2 \left[R_o^2 + \frac{R_s^4}{R_o^2} - 2 \ln R_o \right] \quad ,$$

and

$$(\dot{R})^2 + \omega_L^2 \left[R_o^2 + \frac{R_g^4}{R_o^2} \left(\frac{R_o^2}{R^2} - 1 \right) - 2 \ln \frac{R}{R_o} \right] = 0 \quad . \tag{26}$$

At R_m, where the subscript m denotes either a maximum or a minimum of the beam radius, $\dot{R} = 0$. For the case $R_g = 0$, the calculation of R_m is rather straightforward:

$$R_m^2 - R_o^2 - 2 \ln \frac{R_m}{R_o} = 0 \quad . \tag{27}$$

When $A = 1$ in Equation (25), $R_m = R_e$ and there is no scalloping. If $A \neq 1$, there are two solutions, one of which is $R_m = R_o$. If $A > 1$,

$$R_{max} = R_o \quad ,$$

$$R_{min} = A^2 R_e^2 - a^2 = A^2 - a^2 \quad ;$$

-12-

since $R_e = 1$ and Equation (27) gives

$$a^2 = \ln \frac{A^2}{A^2 - a^2} \quad . \tag{28}$$

For the case of $A < 1$,

$$R_{min} = R_o \quad , $$

$$R_{max} = A^2 + a^2 \quad , $$

where

$$a^2 = \ln \frac{A^2 + a^2}{A^2} \quad . \tag{29}$$

In each of these cases,

$$a^2 = R_{max}^2 - R_{min}^2 = \ln \frac{R_{max}^2}{R_{min}^2} \quad . \tag{30}$$

When $R_g \neq 0$, the calculation of R_m becomes more difficult. It is sufficient for this study to observe the effect on the scallop amplitude of small amounts of flux threading the cathode. From Equation (26),

$$R_m^2 - R_o^2 + \frac{R_g^4}{R_o^2} \left(\frac{R_o^2}{R_m^2} - 1 \right) - 2 \ln \frac{R_m}{R_o} = 0 \quad . \tag{31}$$

It is readily seen that the value $R_m = R_o$ is still a solution for Equation (31). Then Equation (31) may be written as

$$R_{max}^2 - R_{min}^2 + \frac{R_g^4}{R_{min}^2} \left(\frac{R_{min}^2}{R_{max}^2} - 1 \right) = \ln \frac{R_{max}^2}{R_{min}^2} \quad . \tag{32}$$

This requires that for the same difference, $R_{max}^2 - R_{min}^2$, the addition of cathode flux causes the ratio R_{max}/R_{min} to decrease. This means that the

percentage of scalloping decreases, but that the average radius (or equili-
brium radius) increases. It has previously been shown that the effect of
cathode flux is to increase the equilibrium radius over the Brillouin radius.
Thus the effect of flux threading the cathode is to decrease the scallop am-
plitude.

III. CALCULATIONS AND EXPERIMENTAL RESULTS

A. METHODS OF TAKING DATA

The data for this experiment were obtained using the electron beam analyzer described in Appendix A. Because of the construction of the analyzer, it was not possible to obtain data closer than at a plane 6.2 inches from the anode exit. Measurements were therefore taken in a drift region from 6.2 inches to 20 inches from the anode exit. This restriction caused some uncertainties about the behavior of the beam immediately after leaving the anode exit, which are discussed later in the text. In general, however, the beam behavior could be adequately measured in the region available. Figure 20 shows some typical data with the beam cross section as a function of axial position for several values of magnetic field. The beam diameter obtained from data such as are shown in Figure 20 are presented in Figure 2 for five values of magnetic field. This diameter was
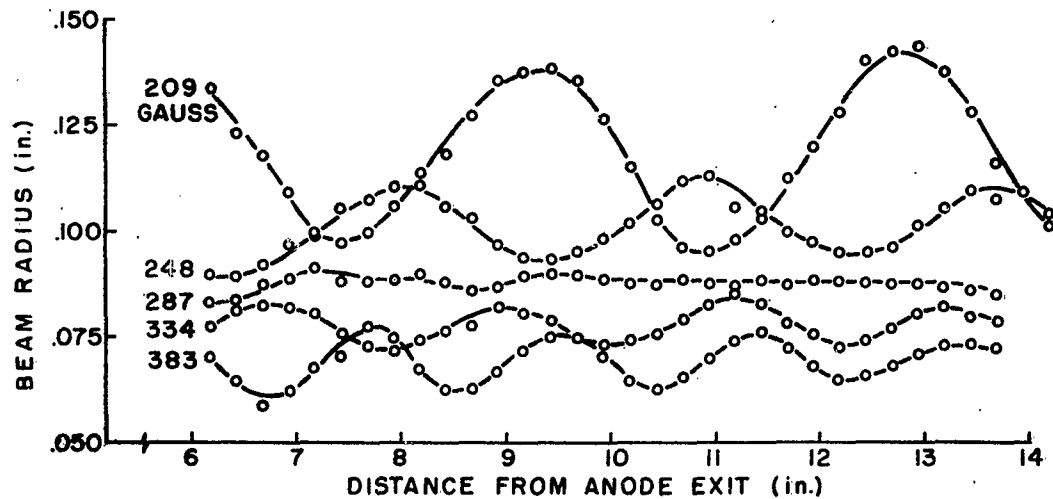
Figure 2. Beam Radius Including 95 Per Cent of the Beam Current versus Axial Position.

measured at the value of current density that was one-third the current

density at the center of the cross section. Detailed measurements on

several cross sections showed that this method of measuring the beam

diameter yielded a value that included 95 per cent of the beam current

within about 1 per cent tolerance.

This method yielded very good results on the beam diameter, but

was very tedious for determining the scallop wavelength for many values

of the focusing field. By measuring the variation in current density on the

axis, one could obtain the scallop wavelength much more easily.

Plots showing the current density variation on the axis are shown

in Figure 3. A unit of J_o in this plot is the current density on the axis

when the beam is focused by the Brillouin field. Figure 3 is a direct

reproduction of data taken on the x-y recorder, on which all data were

recorded. It is apparent that it was easier to measure the scallop wave-

length from these plots than to reduce the data as required for Figure 2.

B. CALCULATIONS OF THE BRILLOUIN FOCUSING FIELD

To calculate the Brillouin field,[*] the current, voltage, and beam

radius must be accurately known. The beam radius is one of the most

difficult parameters of the beam to define because of the finite slope of

the beam edge, which makes it necessary to choose some value of radius

arbitrarily and define it as the beam "edge." For Figure 2 the beam diam-

eter including 95 per cent of the current was chosen. With this value, the

radius of the nonscalloping Brillouin beam was .088 in. Since the beam

_____

[*] In this study the term Brillouin field will refer to the value of focusing
field that produced the minimum scalloping on the Brillouin beam.
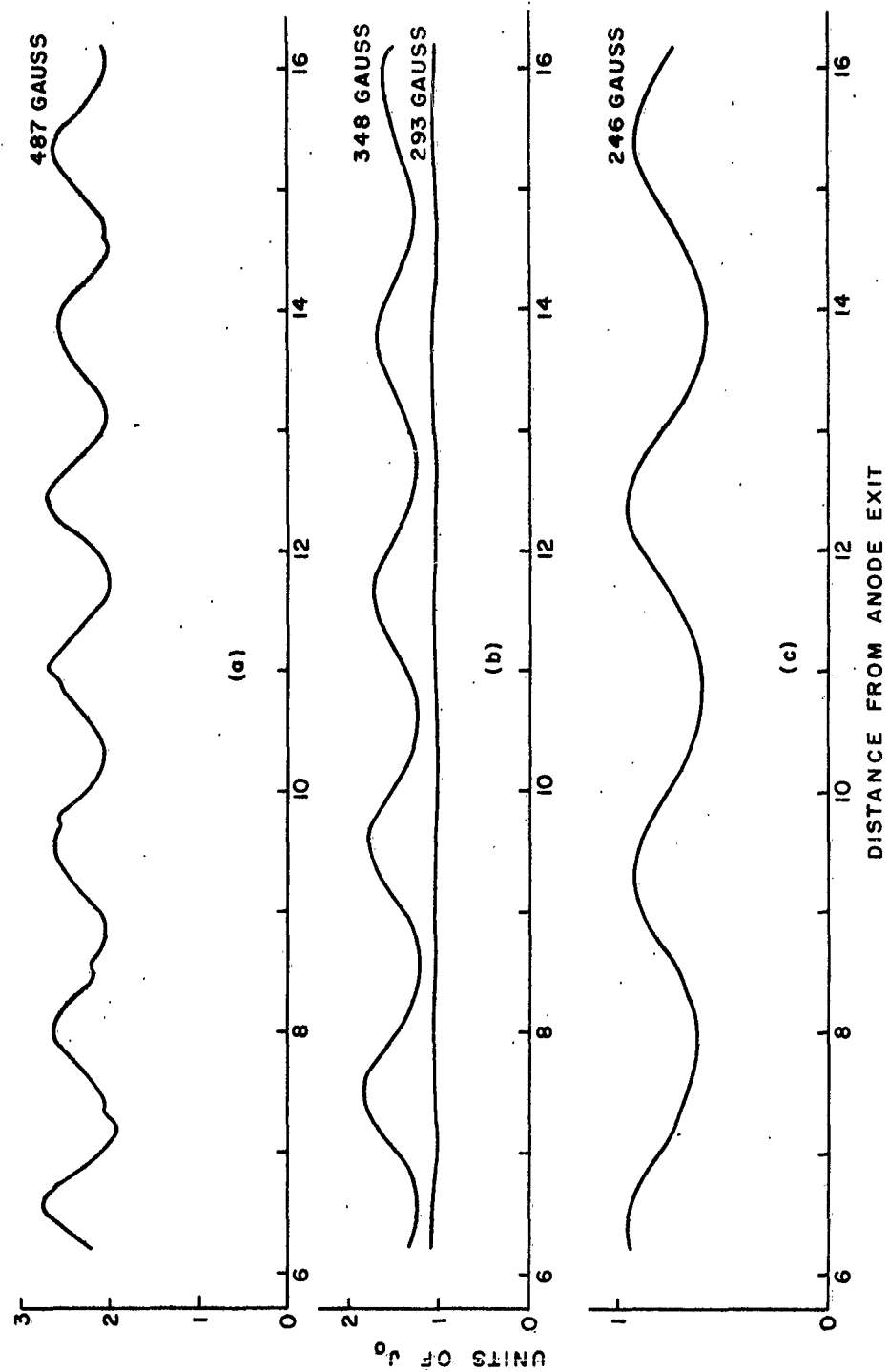
Figure 3.   Current Density on the Beam Axis versus Axial Position.   (The unit of J_o is the current density on the axis when there is no scalloping.)

current and voltage were known, this made it possible to calculate the

Brillouin field using the equation derived by Pierce[5]:

$$I_o = 1.45 \times 10^6 \, B^2 \, V_o^{1/2} \, r^2 \quad \text{(mks)} \quad . \tag{33}$$

For this calculation, the effective voltage, $(V_{eff})^{1/2} = .95 \, (V_o)^{1/2}$, was

used to allow for the depression in potential at the beam center. This cor-

rection was calculated by Gilmour[3] for the perveance and the drift tube

size used. With

$$I_o = .407 \text{ a}$$

$$V_o = .5000 \text{ v}$$

$$r = .088 \text{ in.} \quad ,$$

the calculated value of magnetic field was

$$B = 297 \text{ gauss.}$$

The amplitude of the beam scalloping was less than 5 per cent over a

range of focusing field from 287 to 293 gauss. This indicated an experi-

mental value of the Brillouin field of 290 gauss. This is within 2.4 per

cent of the theoretical value, which is excellent agreement with the theory,

in view of the assumption made in the calculation. Because of this agree-

ment and the limitation on the accuracy of the calculation, a value of

290 gauss is used for the Brillouin field in the following discussion.

Previous experimenters have reported that much higher fields than

the calculated Brillouin value were required to focus the beam.[6,7,8]

Brewer,[6] reported that fields 10-20 per cent greater than the calculated

Brillouin value were required to obtain minimum scalloping. He also noted the presence of a translaminar stream of electrons in his beam caused by aberrations in the anode of the gun. In the beam studied, however, there was very little translaminar motion detected. This suggests that significant amounts of translaminar motion in the beams studied in previous experiments made it necessary to use focusing fields higher than the calculated Brillouin field. This would mean that the optics of the STL-100 electron gun are much better than those usually encountered in electron guns, so that the entrance conditions at the anode exit approximate the theoretical model more closely than in previous experiments, resulting in a more nearly laminar beam.

C. EQUILIBRIUM BEAM RADIUS

In Figure 4 the equilibrium radius, r_e, is plotted as a function of magnetic field, using Equation (17). In these calculations, and in all others in this study, the ratio B_c/B (where B_c is the flux through the cathode) was assumed to be constant for all values of magnetic field, a valid assumption if the shielding material over the electron gun saturated uniformly. In practice B_c/B was probably not constant, but over the narrow range of magnetic field used, this was a reasonable approximation.

When the ratio B_c/B was constant, the term R_g, which accounted for flux through the cathode, could be evaluated in terms of the beam parameters:

$$R_g^4 = \frac{g^4}{a^4} = \frac{r_c^4}{a^4}\left(\frac{B_c}{B}\right)^2 = r_c^4\left(\frac{B_c}{B}\right)^2 B^4\left(\frac{\eta\epsilon_o \pi u}{2 I_o}\right)^2 .$$
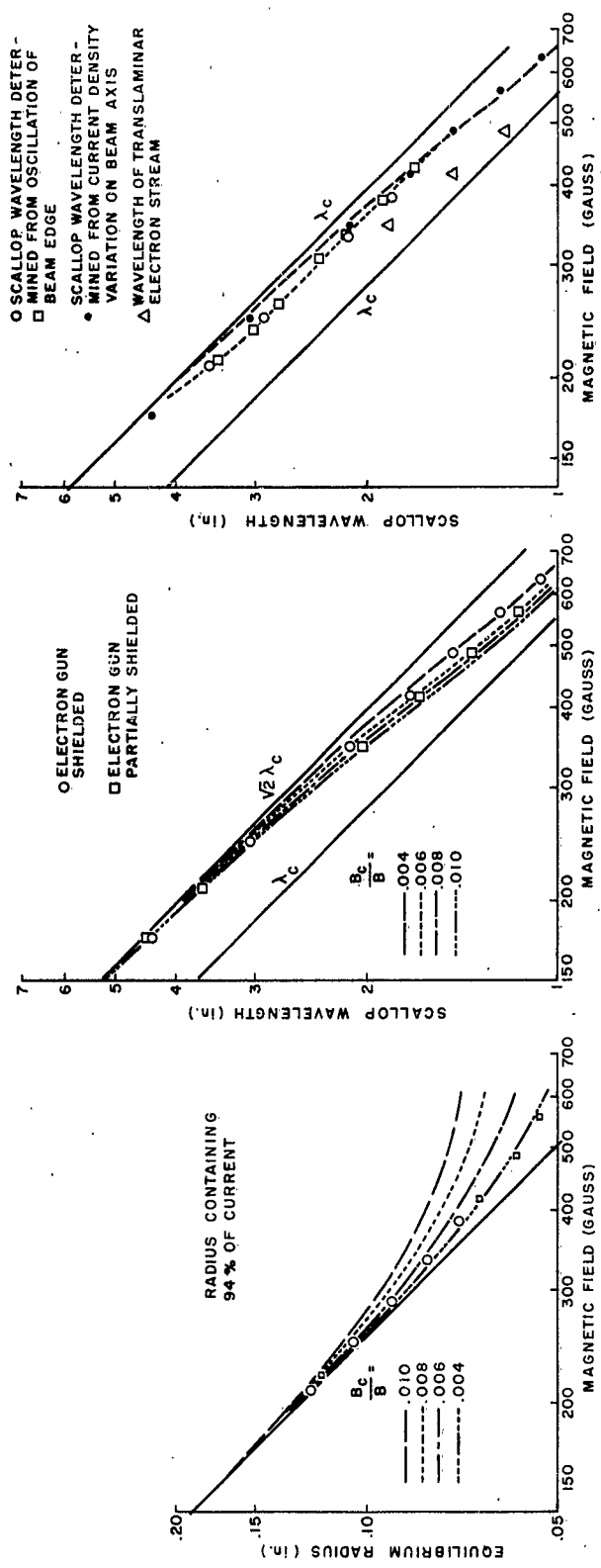
Fig. 4. Equilibrium Radius as Function of Magnetic Field When Small Amount of Flux Threads Cathode.

RADIUS CONTAINING 94% OF CURRENT

$\frac{B_c}{B} =$
.010
.008
.006
.004

MAGNETIC FIELD (GAUSS)

EQUILIBRIUM RADIUS (in.)

Fig. 5. Scallop Wavelength Determined from Current Density Variation on Beam Axis Compared with Laminar Theory.

O ELECTRON GUN SHIELDED
□ ELECTRON GUN PARTIALLY SHIELDED

$\sqrt{2}\,\lambda_c$
λ_c

$\frac{B_c}{B} =$
.004
.006
.008
.010

MAGNETIC FIELD (GAUSS)

SCALLOP WAVELENGTH (in.)

Fig. 6. Comparison of Scallop Wavelength Determined from Beam Edge and Axial Current Density Variations.

O SCALLOP WAVELENGTH DETERMINED FROM OSCILLATION OF BEAM EDGE
□
● SCALLOP WAVELENGTH DETERMINED FROM CURRENT DENSITY VARIATION ON BEAM AXIS
△ WAVELENGTH OF TRANSLAMINAR ELECTRON STREAM

λ_c
λ_c

MAGNETIC FIELD (GAUSS)

SCALLOP WAVELENGTH (in.)

Then if

$$D = r_c^4 \left(\frac{\eta \epsilon_0 \pi u}{2 I_0}\right)^2 \quad ,$$

where D is a constant for a given beam voltage,

$$R_g^4 = D \left(\frac{B_c}{B}\right)^2 B^4 \quad . \tag{34}$$

Since $R_g \sim B$, the value of r_e was tabulated for several values of B for different ratios B_c/B and the appropriate curves drawn. In the calculation using Equation (17), the ratio r_e/a was obtained. The value of effective beam voltage was used in calculating a in a manner similar to that used in calculating the Brillouin magnetic field.

The beam radius containing 94 per cent of the beam was plotted for several values of magnetic field. Data was taken on the beam using two different cathodes in the same gun. Values of r_e obtained from each cathode over different ranges of magnetic field are shown. The radius including 94 per cent of the current was chosen for this plot to obtain the best fit with the theoretical curves. Several values of radius were tried, all of which produced curves of nearly the same shape but different vertical position on the plot. The value of r_e for the lowest magnetic field was most important, since it should have been just above the curve calculated for $B_c/B \cong 0$.

The variation of the equilibrium radius as the magnetic field was increased indicated that $B_c/B = .004$. The presence of this flux is important in explaining some of the anomalies observed by Gilmour[3] and is discussed more fully in a later section.

-21-

D. SCALLOP WAVELENGTH

In Section II it was shown that when the entrance conditions at the anode exit were not those required for Brillouin flow,[*] the beam edge would oscillate radially, so that the beam took on a scalloped appearance. The scallop wavelength was derived from the linearized trajectory equation. This wavelength is plotted in Figure 5 for low values of B_c/B. The general behavior is seen to agree with the behavior predicted in the discussion of the theory. The value of λ_c used in calculating the scallop wavelength was obtained from the beam velocity and magnetic field: $\lambda_c = 2\pi u/\eta B$. The accuracy of this calculation of λ_c has been experimentally verified by Gilmour,[3] who used the effective beam velocity.

Figure 5 shows values of scallop wavelength obtained from measurements, similar to those of Figure 3, of current density on the axis. These values support the observation that there is a fraction of the focusing field threading the cathode and that $B_c/B \cong .004$.

Some further measurements of the scallop wavelength were made with some of the shielding removed from the cathode. In addition to the ferromagnetic gun shell, an iron cap was usually placed over the gun to provide additional shielding. This cap is shown in Figure 13. By removing this cap the amount of flux threading the cathode was increased slightly. The measurements of scallop wavelength shown in Figure 5 indicate that this increase was $B_c/B \cong .002$.

This change in the scallop wavelength obtained by allowing additional flux to thread the cathode supports the view that the decrease in

---

[*]The term Brillouin flow refers to a Brillouin beam focused by the Brillouin field.

scallop wavelength below the theoretical value was indeed due to a small amount of flux threading the cathode. This is important in explaining the anomaly observed by Gilmour.[3] He measured scallop wavelengths 7 per cent shorter than those predicted by theory ($\lambda_s = 1.31 \lambda_c$ instead of $\lambda_s = \sqrt{2} \lambda_c$), but concluded that no flux threaded the cathode because the plot of λ_s versus B had a slope of -1. The basis for this conclusion is shown in Figure 6, where the values of scallop wavelength measured from oscillations of the beam edge are plotted. The points represented by circles are values obtained in this study, and those by squares are values obtained by Gilmour.[3] The agreement between these values is seen to be extremely good, which points to the high accuracy of these measurements.

This high accuracy near the Brillouin value of magnetic field makes significant the marked deviation between values of scallop wavelength measured from the oscillations of the beam edge and those measured from the variation in charge density on the beam axis. This deviation must arise from phenomena not included in the laminar theory. This difference can be explained by considering the motion of a group of translaminar electrons moving in the interior of the beam.

Assume, then, that the theory is valid and that the values of scallop wavelength measured from the current density on the axis are those closest to the correct value, even though near the Brillouin field these values were also lower than predicted by the theory. It should be noted that any phenomenon which alters the scallop wavelength of those electrons near the outer edge of the beam might also affect the wavelength of electrons near the beam axis.

Brewer[6] has shown that for a Brillouin beam that does not scallop, the interior of the beam is a force-free region; that is, an electron moving across the beam in a translaminar manner will not be deflected until it passes outside the beam. For a Brillouin beam with small scallops, the forces on translaminar internal electrons will be small. If there are significant numbers of translaminar electrons, this idealized view would not be valid, but this would be because the laminar electrons had been perturbed from their "perfect" Brillouin trajectories.

Consider the case of a Brillouin beam that is scalloping very slightly, as illustrated in Figure 7. In the interior of this beam is a stream of translaminar electrons comprising only a few per cent of the total beam current. The translaminar stream can be considered to be scalloping with a wavelength shorter than the beam scallop wavelength. Since this translaminar stream is oscillating violently, the forces on electrons in this stream are relatively large, and the wavelength of this stream may be considered to be rather stable. The laminar electrons are oscillating with low amplitudes, where the focusing forces are
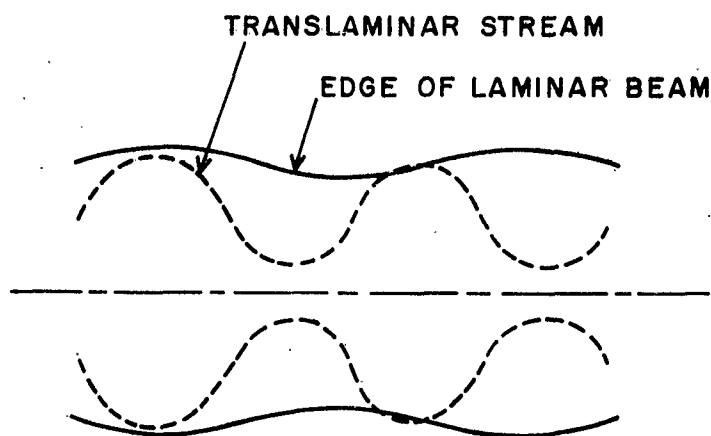

Figure 7. Motion of Translaminar Stream in Brillouin Beam.

delicately balanced, therefore it is quite conceivable that the space-charge forces of the translaminar stream would "pull" the wavelength of the laminar electrons toward the translaminar scallop wavelength. This would appear as a shortening of the beam scallop wavelength. The wavelength of the translaminar stream would also be pulled toward the scallop wavelength of the beam to allow the transverse momentum to be conserved. This pulling effect on the wavelength would be most noticeable near Brillouin flow. Since this translaminar stream is assumed to include only a small per cent of the total beam current, its effect on the wavelength would not be appreciable when the scalloping becomes large.

This hypothesis can now be related to the actual beam studied. At high magnetic fields, a translaminar stream such as the one described was clearly observed in the beam, and cross sections of the beam taken at several axial positions showed that it oscillated violently. The presence of this stream can also be noted in Figure 3a at the points where it passed near the beam axis. At values near Brillouin flow and below, this translaminar stream became too diffused to be identified, but the translaminar electrons should still be present in the beam. The wavelength of the stream was determined at high values of magnetic field and is plotted in Figure 6. A curve drawn through these values would be similar to one plotted from the theory for a rather high value of flux threading the cathode. Near the edge of the cathode the flux threading the cathode would be expected to be higher than the average flux threading the cathode because of the close proximity of the ferromagnetic focusing electrode. Also, Brewer[6] has shown that the electrons near the beam edge are likely to be formed into a translaminar stream by aberrations in the anode aperture.

Thus not only the presence but the origin of this translaminar stream can be identified.

Therefore, near Brillouin flow, translaminar electrons were present in the beam which could disturb the scallop wavelength as hypothesized. For a magnetic field of roughly 200 gauss, i. e., 2/3 the scallop-free Brillouin value, the curve of slope - 1 is seen to turn toward the value predicted by the theory. From the hypothesis this would be expected as the beam scalloping again became large. Because the slight upward trend in the value of scallop wavelength was always observed, it must be considered significant. Furthermore, Gilmour observed this phenomenon occurring consistently at values of beam voltage in the range 3000 v – 6000 v.

The presence of oscillations with two different wavelengths in the beam should result in a beating effect. This was in fact observed; moreover, it was observed only for focusing fields near the Brillouin field. Because of the small amplitude of the beam scallops in this region, it was difficult to observe, but it was observed by measuring current density variation on the axis with high level of gain in the recording circuitry.

It may be safely concluded, therefore, that the translaminar electrons in the beam had caused part of the reduction in scallop wavelength observed by Gilmour. Of the 7 percent error, about 3 percent may be attributed to the presence of flux threading the cathode and the remaining 4 percent to the pulling effect of the translaminar electrons.

It has been shown that when flux threads the cathode, the translaminar stream cannot pass through the beam axis. Since the primary effect of this stream must be on electrons in the region through which it moves, this explains why the scallop wavelength measured from the current

density variation on the beam axis should differ from that measured at the beam edge. The slight decrease in scallop wavelength on the beam axis below the theoretical value may be ascribed to the secondary effect of the wavelength of the outer edge scallop pulling the axial scallop wavelength.

Some other properties of the translaminar stream should be noted:

1. The reason the translaminar stream appears in Figure 3a is that the pin-hole of the scanner was not exactly on the beam axis. This was because the beam axis oscillated about the axis of the drift tube at the cyclotron wavelength. At some axial positions where the stream would have been expected to appear, it was not seen because the pin-hole was on the beam axis.

2. The translaminar stream discussed here was not a part of the tails that have been observed moving transversely in the beam.[3] The scallop wavelength of an electron that makes up part of the tails is nearly that of the beam and therefore would not fit into the explanation of the shortened scallop wavelength.

3. The translaminar stream referred to here is definitely a property of the STL-100 gun and not the result of a cathode imperfection or misalignment of one particular cathode. It was observed on the beams generated from several cathodes.

E. MAGNITUDE OF BEAM SCALLOPS

The magnitude of the beam scallops computed from Equation (30) is plotted in Figure 8. The radius including 95 per cent of the beam and the radius of the outer edge of the beam are shown on the plot. The outer edge of the beam was determined by extrapolating the side of the beam to zero current as shown in Figure 9. Neither of these values of the radius
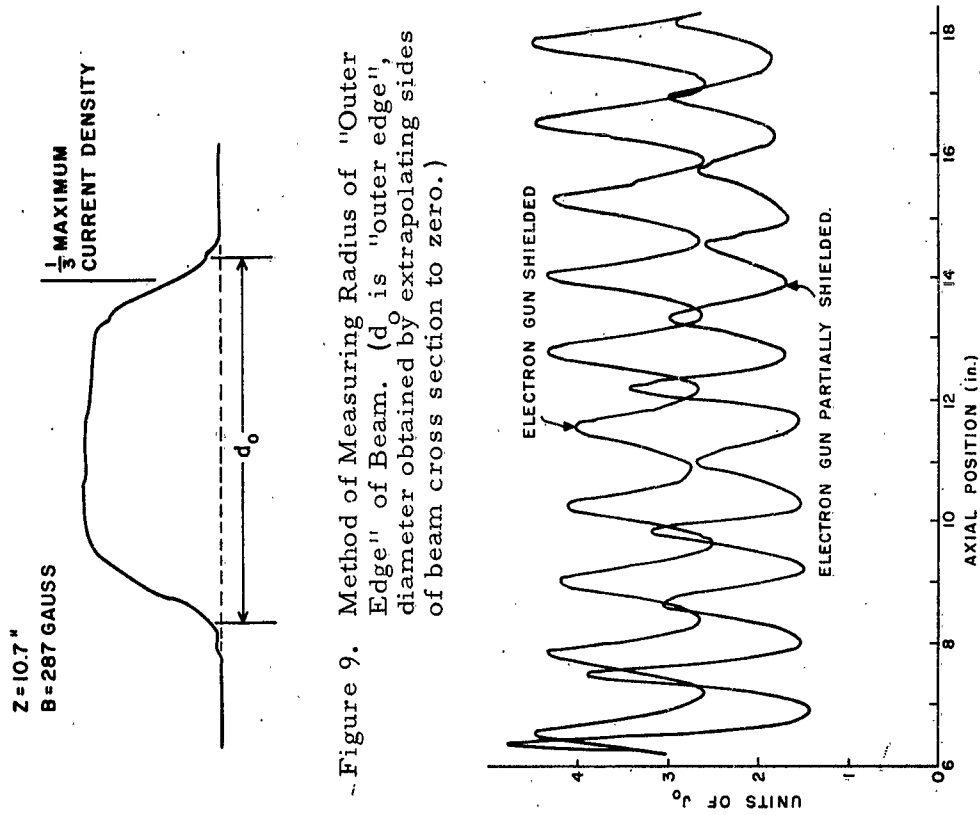
Figure 9. Method of Measuring Radius of "Outer Edge" of Beam. (d_o is "outer edge", diameter obtained by extrapolating sides of beam cross section to zero.)
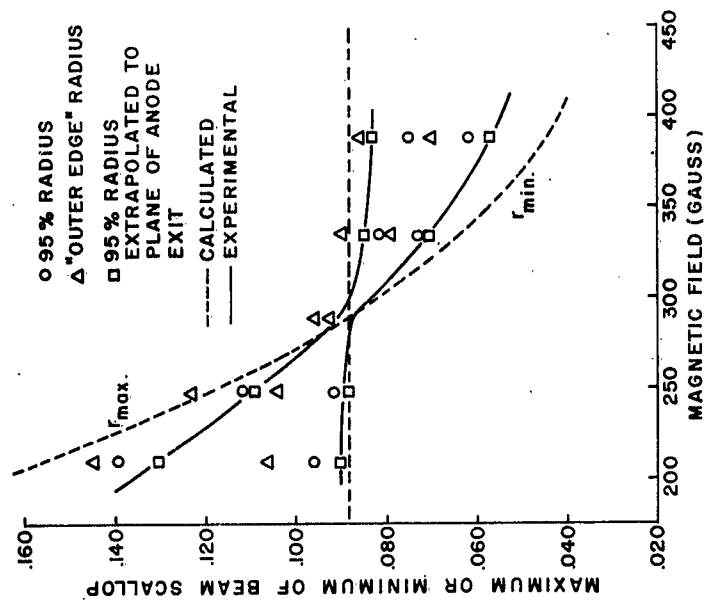

Figure 10. Effect of Flux through the Cathode on Current Density on the Beam Axis.

Figure 8. Magnitude of Beam Scallops as Magnetic Field is Varied.

provides a good fit with the theory for magnetic fields either above or below the Brillouin field of 290 gauss.

This discrepancy can be resolved after careful examination of Figure 2, which shows that the amplitude of the scallops decreased and the equilibrium radius of the beam increased as a function of axial position. Somewhat better correlation between the theory and experiment was obtained by a linear extrapolation of the measured values of the maximum and minimum radii of excursion back to the plane of the anode exit. There is of course no particular justification for using a linear extrapolation or even the same extrapolation for all values of maxima and minima, but this extrapolation points up the problem. A good fit between the maximum and minimum radius of the beam scallop was not obtained, because it was not possible to determine the amplitude of the initial scallop.

This decrease in the magnitude of the scallops and increase of equilibrium radius had been observed by Rigrod[9] and used to explain the growth of noise in the beam. He considered the mechanism for this noise growth to be scalloped beam amplification, in the manner described by Mihran.[10] It is possible that this phenomenon could be used to explain the decrease in magnitude of the beam scallop observed here.

F. ACCURACY OF THE LINEARIZED THEORY

Striking confirmation of the validity of the linearized theory for the region of interest was obtained using the data presented in Figure 10. In this figure data similar to that shown in Figure 3 was obtained with and without the shielding cap over the electron gun. The average axial current

was reduced by approximately 28 per cent when some of the shielding was removed. If the beam shape remains constant (variation of P with radius does not change), then

$$\frac{\Delta J_o}{J_o} = \frac{(\Delta r_e)^2}{(r_e)^2} \quad , \tag{35}$$

and the decrease in axial density corresponds to an increase in the equilibrium radius of 13 per cent. From Figure 4, this corresponds to an increase in equilibrium radius to 0.61 in. or $B_c/B \cong .006$. This value of flux threading the cathode when the shielding cap was removed is the same as that obtained in direct measurements. This agreement attests to the accuracy of the measurements and the soundness of the theory.

G. THERMAL EFFECTS

It is well recognized that the assumption of a laminar beam is highly idealistic. In a true laminar beam the electrons must have zero velocity at the cathode, whereas, in fact, the electrons are emitted in random directions with a wide range of velocities. Thus despite the excellent agreement noted between the laminar theory and the over-all beam behavior, some differences in the details of electron motion are to be expected.

It is characteristic of electron beams that the beam edge is not sharp, as predicted by the laminar theory. This arises from the transverse velocities of the thermal electrons which cross the nominal beam edge and cause this edge to appear diffuse. Pierce and Walker[11] have derived a theory that incorporates a thermal correction into the laminar theory. They assume that the transverse velocities of the electrons are

in thermal equilibrium with a Maxwellian distribution of charge density within the beam. In their derivation, Pierce and Walker derive a factor, μ, which is proportional to the beam parameters:

$$\mu = 5.56 \frac{I_o}{T_o \sqrt{V_o}} , \qquad (36)$$

where

I_o = beam current in milliamperes,

V_o = beam voltage in kilovolts,

T_o = beam temperature in hundreds of degrees Centigrade.

It has been observed both theoretically and experimentally[12] that T_o may be calculated by

$$T_o = M^2 T_c , \qquad (37)$$

where M^2 is the area convergence ratio of the gun, and T_c is the cathode temperature.

The fraction of the beam outside a selected radius has been plotted for various values of μ. This plot is reproduced for three values of μ in Figure 11. Using the known beam and gun parameters for a beam voltage of 5000 volts gives

$$\mu = 21.3 .$$

This indicates that the "cold" Brillouin radius (for which $T_o = 0$) would include 90 per cent of the current, but this would require a value of Brillouin field much higher than the experimental value; therefore the 95 per cent radius must be the "cold" radius, and the value of μ must be adjusted to $\mu = 100$.
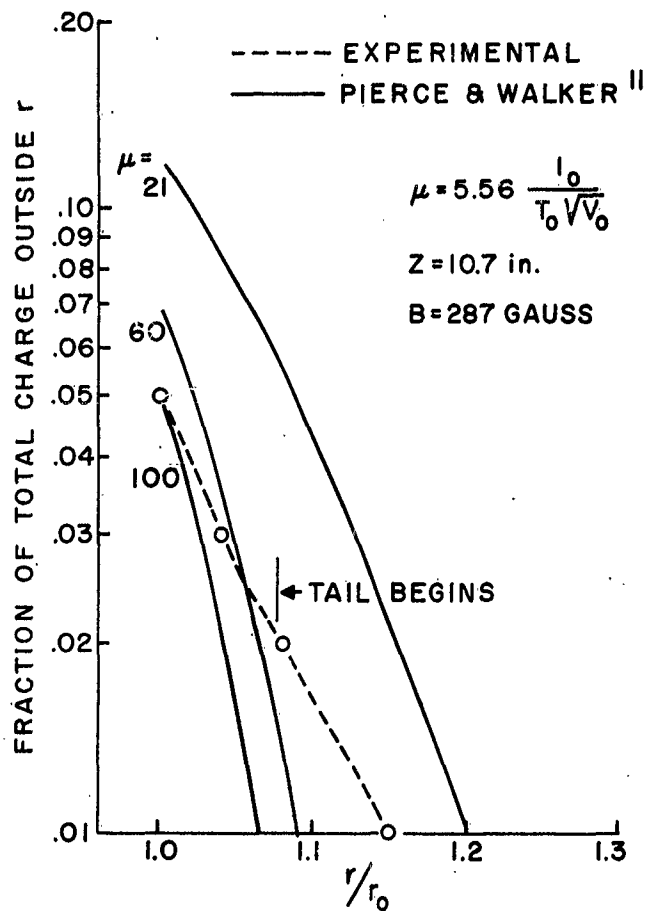
Figure 11. Fraction of Charge Outside of Given Radius, r, Normalized to "Cold" Brillouin Radius, r_0.

The shape of a beam edge obtained from a typical cross section is also shown in Figure 11. In view of the crudeness with which the data points were taken, the correspondence with the Pierce-Walker theory is good. The most significant result is that the observed beam temperature using the "cold" radius was five times lower than that predicted from the Pierce-Walker theory and from Equation (6). The reason for this is not fully understood.

Another theory that has been proposed to describe the thermal velocity effects in the beam is Herrmann's optical theory.[13] The electrons are assumed to move in a perfect optical system under the paraxial-ray assumptions, and the requirement of laminarity is discarded. The beam is shown to form corssovers and images at successive points on the axis. At a crossover the beam cross section is Gaussian in shape, and at an image the beam cross section is rectangular (an image of the cathode). This theory also predicts that the focusing field should be larger than that predicted by the laminar theory as given in Equation (33).

Electron flow like that predicted by the optical theory has been observed experimentally under special conditions;[7] i.e. at low voltage, where thermal effects become very significant. In this study the STL-100 gun was also operated at low voltage – 420 volts – to see if a correlation between the beam behavior and the optical theory could be obtained. This data is shown in Figure 12a and can be compared with the data obtained at 5000 volts as shown in Figure 12b.

The beam edge is much more diffuse in Figure 12a than in Figure 12b. The thermal theory of Pierce and Walker predicts this. From Equation (36) for a beam of constant perveance, K,

$$\mu \sim \frac{I_o}{T_o V_o^{\frac{1}{2}}} = \frac{K V_o}{T_o} , \qquad (38)$$

so that μ is directly proportional to the beam voltage. Using the value already obtained of $\mu = 100$ at 5000 volts, we get $\mu = 8.4$ for 420 volts, and from Pierce and Walker's results, the "cold" Brillouin radius is found to include only 80 per cent of the beam current. This accounts for the diffuse beam edge. The optical theory does not provide a means for determining

HORIZONTAL POSITION IN BEAM (INCHES)
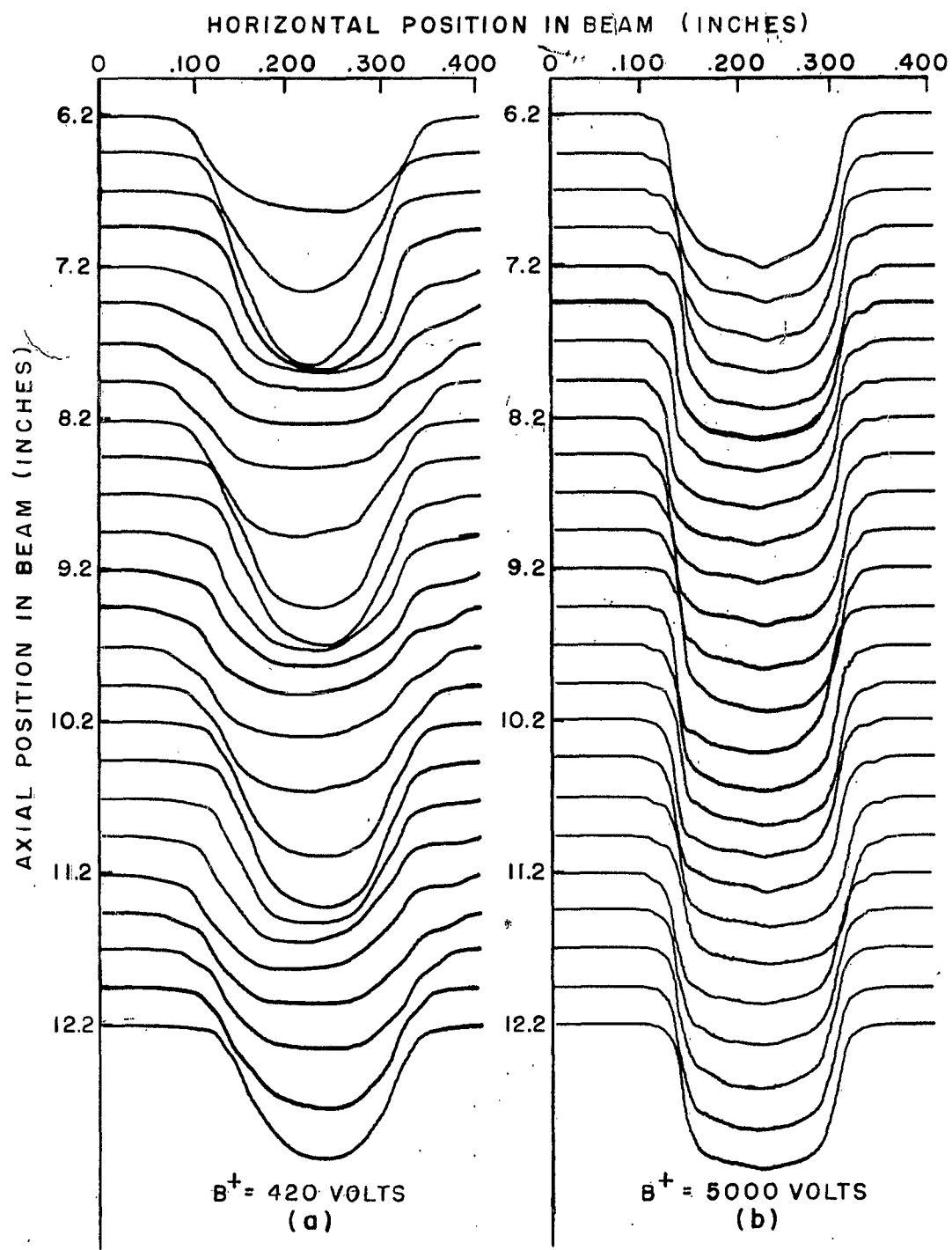
B⁺ = 420 VOLTS
(a)

B⁺ = 5000 VOLTS
(b)

Figure 12. Beam Cross-Sections Showing Applicability of Optical Theory.

the beam edge. Since the beam edge is diffuse, one must be able to determine the nominal beam edge; therefore the 80 per cent radius obtained from Pierce and Walker was used.

When the beam radius that included 80 per cent of the beam was plotted, it was found that this radius scalloped about the value $r_e = .087$ in., which is essentially the same as the "cold" Brillouin radius determined at a beam voltage of 5000 volts. Ideally the beam edge should not scallop at this radius. It was shown in an experiment at 5000 volts, however, that beam scalloping of considerable magnitude could readily be induced by moving the magnetic pole piece axially 1/8 in. This changed the entry conditions at the anode exit so that they deviated from ideal conditions, which would indicate that the scalloping of the beam edge at 420 volts may be attributed to improper entry conditions.

Except for the diffuse beam edge and scalloping, the beam was seen to follow the predictions of the optical theory. The fact that Gaussian crossovers were formed periodically is not entirely evident from the data in Figure 12a because of the distortions arising from the beam scalloping. A scallop wavelength of $1.19 \lambda_c$ was measured, which could be compared to the distance between images of $1.6 \lambda_c$. It was not possible to adjust the focusing field so that the current density on the axis did not vary, as would be expected from the model of the optical theory.

The validity of the laminar and optical theories for the low-voltage beam is compared in the following table. The values calculated from the optical theory were obtained using Equation (5) instead of the corrected beam temperature needed for the Pierce and Walker theory, and are shown in Table I.

-35-

TABLE I

Comparison of Optical and Laminar
Theories with Experimental Measurements

Value	Measured	Laminar Theory	Optical Theory
B (gauss)	107	84	108
λ_s/λ_c	1.19	1.41	1.21

The beam behavior at 5000 volts does not agree with the optical theory model. A calculation using this theory predicts a required focusing field of 306 gauss, which is somewhat high. Much more serious is the difference in the beam cross section and the prediction of periodic crossovers of Gaussian shape. The data in Figure 12b show no such tendency. When similar data were taken over the full range of from 6.2 in. to 20 in. from the anode exit, no change in the beam cross section was noted. This also held true when the beam was scalloping with radial variations of up to 40 per cent. A calculation from the optical theory predicts that crossovers should occur every 10.2 in., so that at least one cross over should have occurred within the space in which data was taken. The assumptions under which the optical theory was derived do not seem to have been violated, so it would seem that the model is not valid at high voltages.

IV. DISCUSSION AND CONCLUSION

A. SUMMARY OF RESULTS

The linearized theory of the laminar beam presented has been shown to predict the beam behavior near Brillouin flow accurately even when a small amount of flux threads the cathode, which indicates that the laminar model gives a close representation of the behavior of the medium-power beam. The observed correlation between separate measurements on the beam, which was predicted by the theory, indicates that the data taken in this experiment are of high accuracy.

The optical model of the beam, which has been proposed to allow for the thermal velocities of the electrons, was shown to be very accurate at low beam voltage (420 volts), but not valid at the higher voltages usually used with this beam. At higher voltages the beam was focused at the calculated Brillouin field and the periodic appearance of Gaussian cross sections in the beam was not observed, as would be expected from the laminar model. Therefore, the laminar model is a closer representation of the actual beam behavior at higher voltages. This is not very surprising, since at higher beam voltages the thermal effects become relatively smaller. It has not been previously reported that the optical theory is not applicable at higher voltages. It should, therefore, be restricted in its application to devices operating at low beam voltages.

The linearized theory developed in this report has wider application than the theory used by Gilmour[3] in that the restriction $R_g \ll 1$ has been removed. For a gun of high area convergence, such as the one used in the

STL-100, this restriction can be shown to make Gilmour's theory invalid even when B_c/B is only a small fraction of one per cent.

The anomaly in the scallop wavelength observed by Gilmour was also observed in this experiment. In addition it was observed that the scallop wavelengths measured on the beam axis near Brillouin flow differed from those measured on the beam axis. This behavior has been attributed to a translaminar stream moving near the outer edge of the laminar beam that "pulled" the scallop wavelength of the outer edge electrons when the focusing field was near the Brillouin field. Gilmour's finding that a straight line of slope -1 best fit his data points, indicating an observed scallop wavelength less than the calculated value, must be attributed to his data being taken over a narrower range than reported here.

The anomalous magnitude of the beam scallop has been shown to be due at least in part to the data not being taken in the region where the beam entered the magnetic field and to the scallop decreasing with axial position from the anode exit to the region where data were taken. This decrease in the magnitude of the scallop cannot be explained using the laminar theory but may be due to noise amplification in the beam as described by Rigrod.[9]

The diffuse appearance of the beam edge was shown to result from thermal spreading of the electrons across the nominal beam edge as predicted by Pierce and Walker.[11] This agrees with the results of a much more thorough investigation by Brewer,[6] except that an equivalent beam temperature of only one-fifth of the value usually taken[12] was required to obtain this agreement. The reason for this discrepancy is not known at this time.

-38-

B. PROPOSALS FOR FUTURE INVESTIGATION

An investigation of the beam flow in the first six inches after leaving the anode exit should be made. This should make it possible to determine the magnitude of the beam scallops at the anode exit, and the experimental results could then be compared with the maximum and minimum of the scallops predicted by the laminar theory. The shape of the beam edge at several axial positions starting with the anode exit should be compared to the shape predicted by the Pierce and Walker theory. It may be that this theory accurately predicts the beam shape at the anode exit when the calculated value [12] of the beam temperature is used. It does not predict the beam shape in the drift region, where one-fifth of the calculated beam temperature was used. A possible change in beam temperature between the two regions may be related to the decrease in the magnitude of the scallops. Such a change in temperature with distance is not predicted by the Pierce and Walker theory, it would probably be necessary to study the axial variation in transverse noise velocities in the beam to explain it.

A bucking coil should be used with the STL-100 gun to investigate the validity of the linearized laminar theory when appreciable amounts of flux thread the cathode. It would also be of great interest to see if the beam used in these studies can be made to behave as an immersed beam, as this would greatly extend the usefulness of this gun for r-f studies on the Cornell beam analyzer.

APPENDIX A. BEAM ANALYZER

The beam analyzer used in obtaining the data in this experiment was first described by A. S. Gilmour[3] and is shown in Figure 13. This appendix reviews the important features of this analyzer and describes the improvements that have been made since Gilmour's report was published.

A. VACUUM SYSTEM

A schematic diagram of the vacuum system of the analyzer is shown in Figure 14. This vacuum system was designed to meet two criteria: (1) that high ultimate vacuum approaching that found in high-power microwave tubes be attainable, and (2) that it be possible to open, close, and evacuate the system easily and quickly.

The most important improvement made in the primary vacuum system in the course of the experiment was the replacement of the oil diffusion pump system with a 75 l/sec VacIon pump. This ion-getter pump provided several advantages over the old system: faster pumpdown, lower ultimate pressure, reliability, and no oil contamination.

1. <u>Faster pumpdown.</u> Because of the size of the beam analyzer, it was not feasible to bake it while it was being pumped, so that in order to obtain a high vacuum, it was necessary to pump the gas that was slowly evolved from the analyzer parts. The speed of the new pump was estimated to be four to five times that of the oil diffusion pump previously used. Furthermore, the necessity of baking the zeolyte trap before turning on the oil-diffusion pump has added a few hours to the pumpdown process. The result was that with the new pump, pressures in the low 10^{-7} mm Hg range were achieved in a few hours, where 3 - 5 days had been required with the oil-
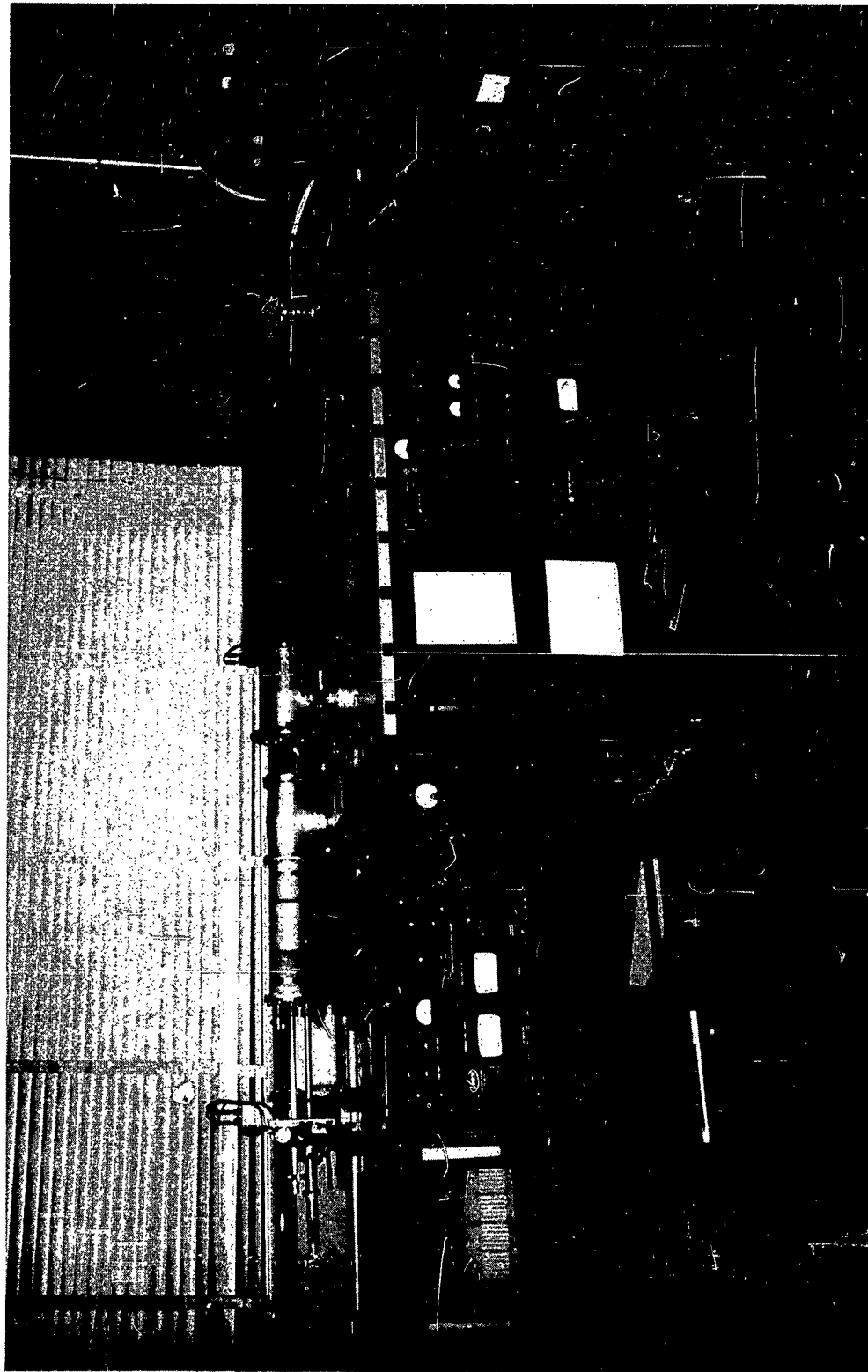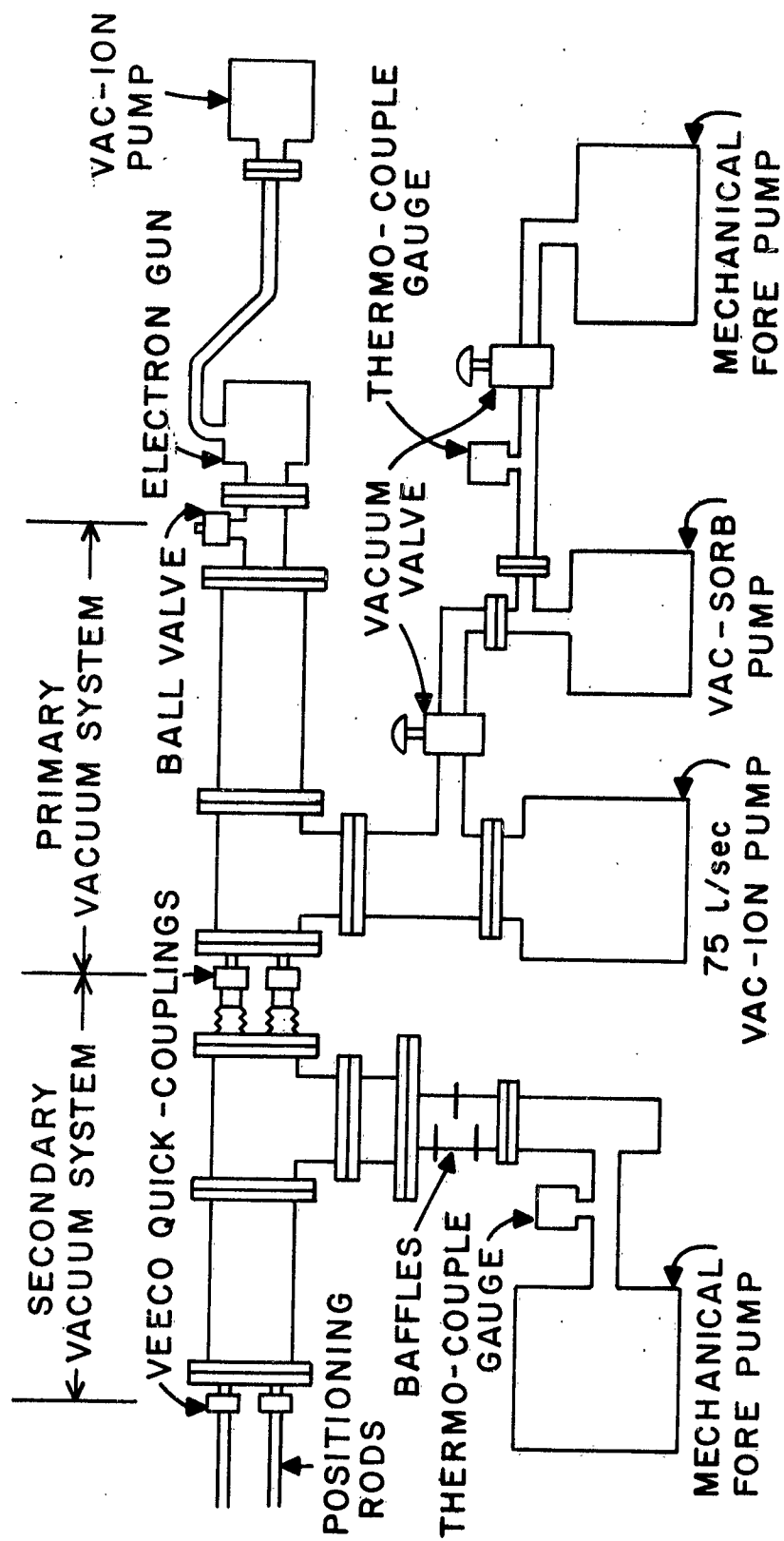
Figure 13. Beam Analyzer.

Figure 14. Vacuum System of Beam Analyzer.

diffusion pump, the length of time depending on the cleanliness of the vacuum system when pumpdown began.

2. <u>Lower ultimate pressure</u>. With the oil-diffusion pump, the best vacuum obtained was a little better than 1×10^{-7} mm Hg; whereas with the new pump, a pressure of 2×10^{-8} mm Hg was achieved in the analyzer, an improvement of nearly an order of magnitude in ultimate pressure. This proved to be significant, since it was found that ions affected the focus of the electron beam.[*]

3. <u>Reliability</u>. When the oil pump was used, electrical and mechanical failures resulted in a loss of vacuum and the spraying of oil from the diffusion pump into the analyzer. This made it necessary to dismantle and clean the analyzer with a consequent loss of several days before the system was pumped down again . While an electric power failure would cause the VacIon pump to stop, it could be restarted, and within a few hours the analyzer would be in operation, since no cleaning would be required.

4. <u>No oil contamination</u>. Even without a power failure, there was a slow but steady backstreaming of oil into the drift tube of the analyzer, which condensed on the scanning mechanism, r-f structure, and walls of the drift tube. With the ball valve open, this oil drifted into the gun region, contaminating the cathode, and thus significantly reducing cathode emission.[1]

The moving parts inside the vacuum system were controlled by polished stainless steel rods sliding through Veeco quick-couplings. These rods were coated with a film of Dow-Corning high-vacuum grease as a lubricant. When the beam was on and data was being taken, it was necessary to move these rods in and out of the primary vacuum system. When the

---

[*] A report on this study has been issued since this report was written: A. S. Gilmour and D. D. Hallock, "Ion Effects in a Brillouin Beam, " Research Report EE 545, Cornell University, 20 October, 1962.

rods were pulled out into the atmosphere, gas was absorbed on their sur-face. This gas was released when the rods were pushed into the system. In order to keep this effect to a minimum, a secondary vacuum system was used to keep those parts of the rods that were to be moved into the primary vacuum system at a pressure of less than 10 microns when they were pulled out of the drift tube. Under these conditions, when the rods were pushed slowly into the vacuum system, only a small change in pressure was obser-ved with the drift tube in the 10^{-8} mm Hg range.

The flanges used in the beam analyzer were designed for simplicity. They were made from No. 304 stainless steel and polished on the mating sides. Two kinds of gaskets were used. Lead O-rings were used for those seals where no insulation was required between mating sections, and when properly installed these gaskets did not leak. It was necessary to tighten these gaskets periodically after they were first installed, because they tended to creep. Their melting temperature of 180 degrees Centigrade prevented high-temperature bakeout, but this was no problem, since good pressures were obtained without bakeout.

When insulation was required between flanges, teflon gaskets were used. In addition insulating sleeves were placed around the bolts and in-sulating washers were placed under the bolt heads. These teflon gaskets were reusable for an indefinite period of time.

One of the most important features of the beam analyzer was the high-vacuum ball valve used to isolate the electron gun from the primary vacuum system. A sketch of the ball valve is shown in Figure 15. When the valve was open, the beam passed through the aperture in the ball. When the valve was closed, the drift tube could be opened to atmospheric pressure

-44-

SHAFT FOR TURNING BALL

VEECO QUICK COUPLING

BALL

TO DRIFT TUBE ←

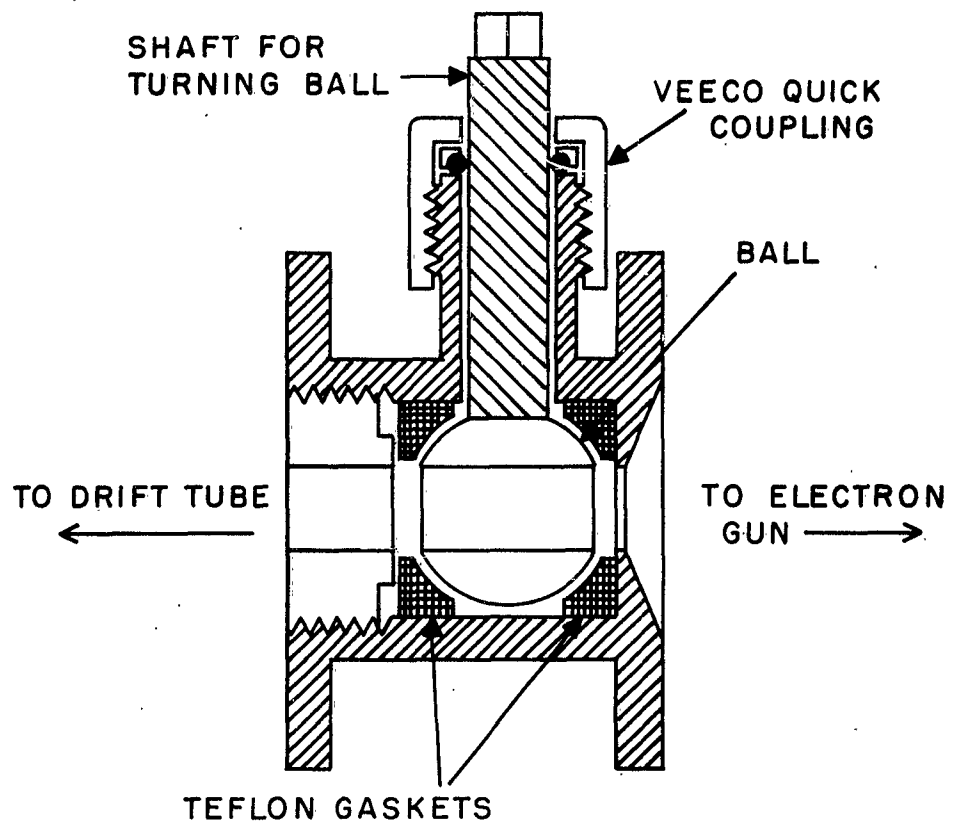TO ELECTRON GUN →

TEFLON GASKETS

Figure 15. Simplified Sketch of Ball Valve with Ball in Open Position.

while the cathode was kept in a high vacuum. The ball, teflon gaskets, and body shell were obtained from a Jamesbury ball valve. The valve, as modi-fied at Cornell University, was capable of holding the gun at pressures about 5×10^{-9} mm Hg. To obtain this performance, however, it was necessary to lubricate the teflon gaskets. Dow-Corning high-vacuum grease was used for this lubrication.

B. ELECTRON GUN

The electron gun used for this experiment was taken from an STL-100 traveling-wave tube.[*] This is a Pierce gun with a perveance of 1.15×10^{-6}, and area convergence of 52.7, at Brillouin flow. It was designed to operate at 5400 volts, but tests were made with this gun at beam voltages of 1000 $\approx$ 10,000 volts with satisfactory results. A photograph of the gun mounted on the beam analyzer is shown in Figure 16.

Mating flanges, similar in design to those used on Varian VacIon pumps were brazed to the gun body and back plate, so that the gun could be readily opened if necessary. A flange that mated with the ball-valve flange was brazed to the gun where it had been cut away from the interaction region of the traveling-wave tube. Provision for pumping the gun when the ball valve was closed was made by attaching an 8 l/sec VacIon pump to the fitting that had served as the exhaust port on the original tube.

Although the electron gun from the STL-100 was capable of d-c operation at 5400 volts, it was necessary to pulse this gun on the beam tester to reduce the power dissipated by the scanning mechanism. The duty cycle was usually .001. A Manson Laboratories modulator capable of supplying up to 20 kv and 20 amperes at a duty cycle of .001 was used to supply the beam voltage.

The heater of the STL-100 gun was operated from a 60-cps sinusoidal supply. When the beam was pulsed at an arbitrary repetition rate, the cathode therefore being pulsed at various values of heater current, Gilmour[3] observed a great deal of modulation on the beam. He attributed

---

[*]This was one of five donated to the School of Electrical Engineering by the Sperry Gyroscope Company.
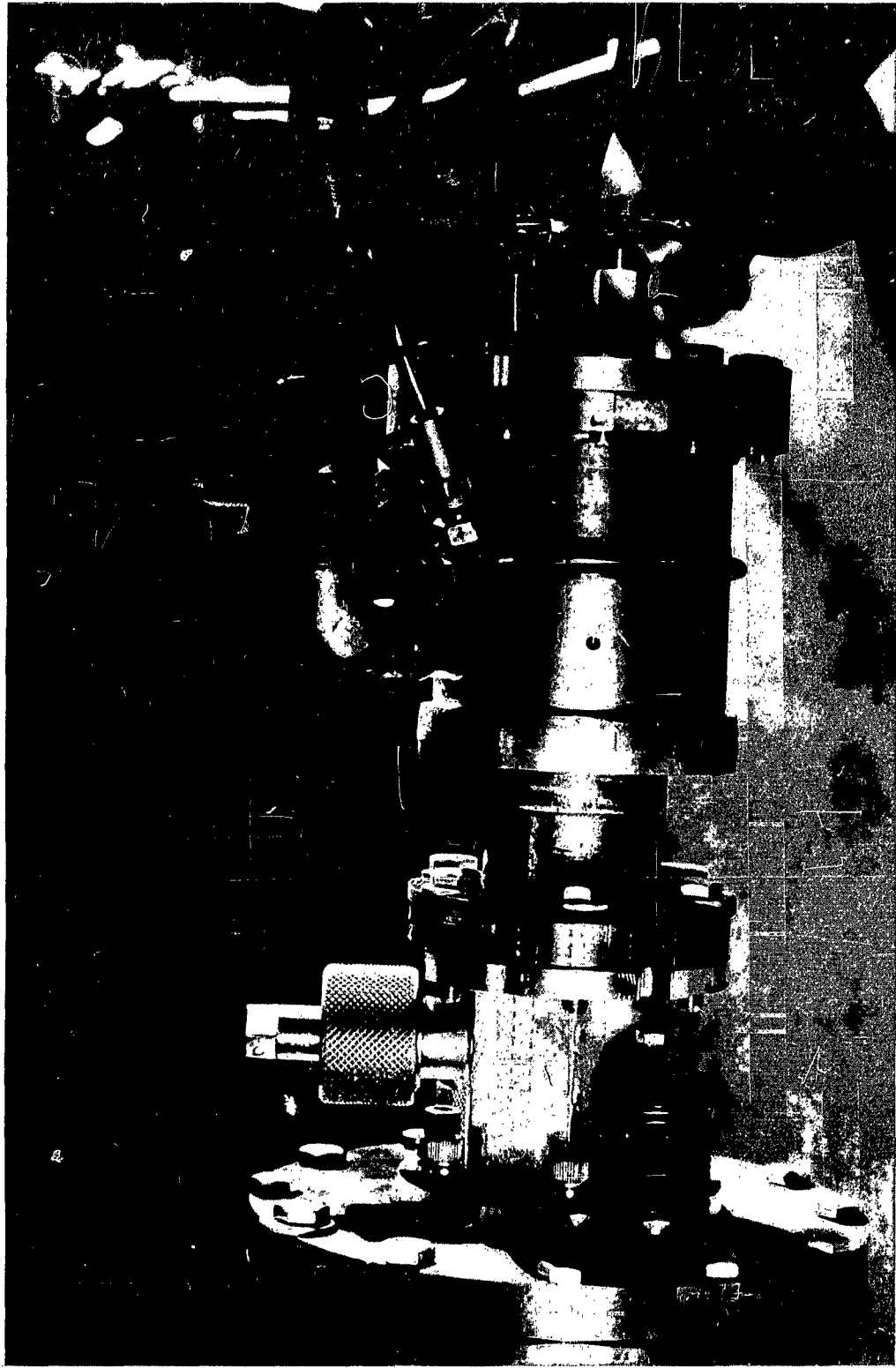
Figure 16.   Electron Gun and Ball Valve Mounted on Beam Analyzer.

this modulation to the magnetic field produced by the noninductive heater used in the gun. When the cathode was pulsed at a repetition rate of 60 cps and the pulses synchronized with zeros of the heater current, thus modulation was eliminated, and the laminarity of the electron flow in the beam was greatly improved.

C. BEAM SCANNER

The electron beam was collected on a pin-hole scanner, which was positioned in the x, y, and z directions in the drift tube. A simplified sketch of the scanner is shown in Figure 17. The beam-collecting area on the scanner was a molybdenum plate that was carbonized to reduce the emission of secondary electrons. A .005-inch hole in the center of this plate allowed a small fraction of the beam to pass through the collecting
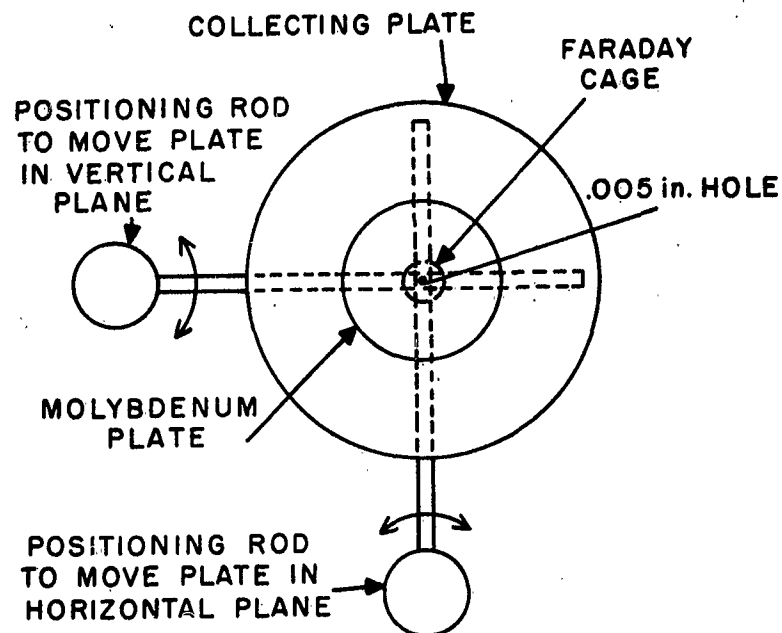

Figure 17. Simplified Sketch of Beam-scanning Mechanism inside Drift Tube.

plate to a Faraday cage. A photograph of the complete scanner is shown in Figure 18. In the beam scanner used for this experiment, the Faraday cage was part of the center conductor of a co-axial line so that injected r-f currents could be measured for other experiments. This, of course, had no effect on its use for d-c measurements.

The scanner was moved by two positioning rods that were controlled from outside the vacuum system. A plate to center the scanner inside the drift tube was attached to these rods behind the collecting plate. The centering plate moved along a guide rail inside the drift tube and was held in position by spring-loaded teflon blocks.

The control mechanism for the positioning rods in shown in Figure 19. The scanning mechanism was moved axially by using the gear and rack arrangement shown in the figure. The angular position of the rods was adjusted by means of the micrometers. The micrometer that set the horizontal position of the scanner was equipped with a motor drive, and reversing switches caused the motor to sweep the scanner back and forth across the beam automatically. A ten-turn helipot was geared to the motor to provide a voltage proportional to the horizontal position of the scanner; this voltage could be applied to the x input of an x-y recorder. The current from the Faraday cage produced a voltage drop across the input resistor of the General Radio electrometer and provided a y input to the recorder proportional to the current to the Faraday cage. Beam cross sections obtained in this manner are shown in Figure 20. From this data the beam diameter could be determined as a function of axial position.
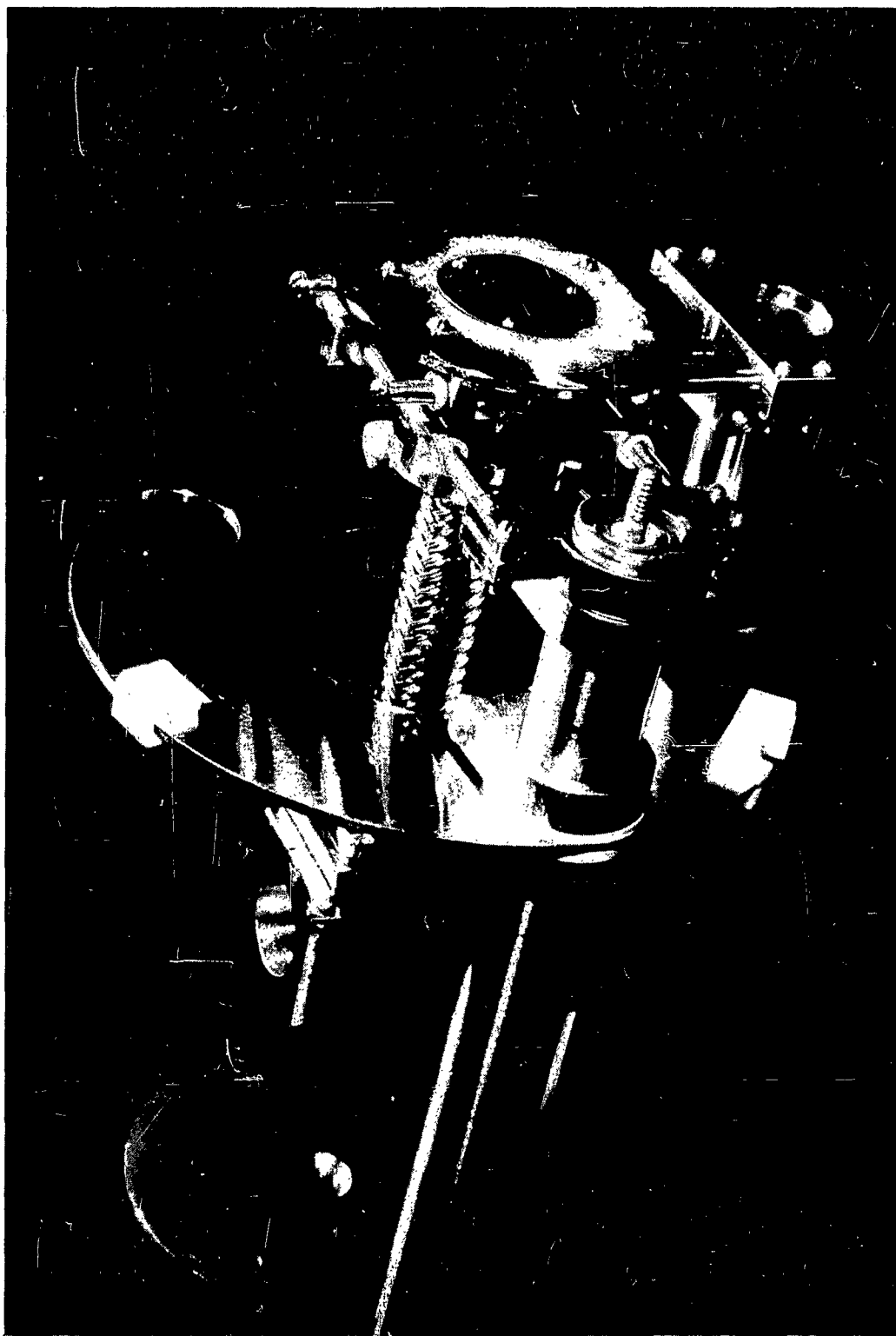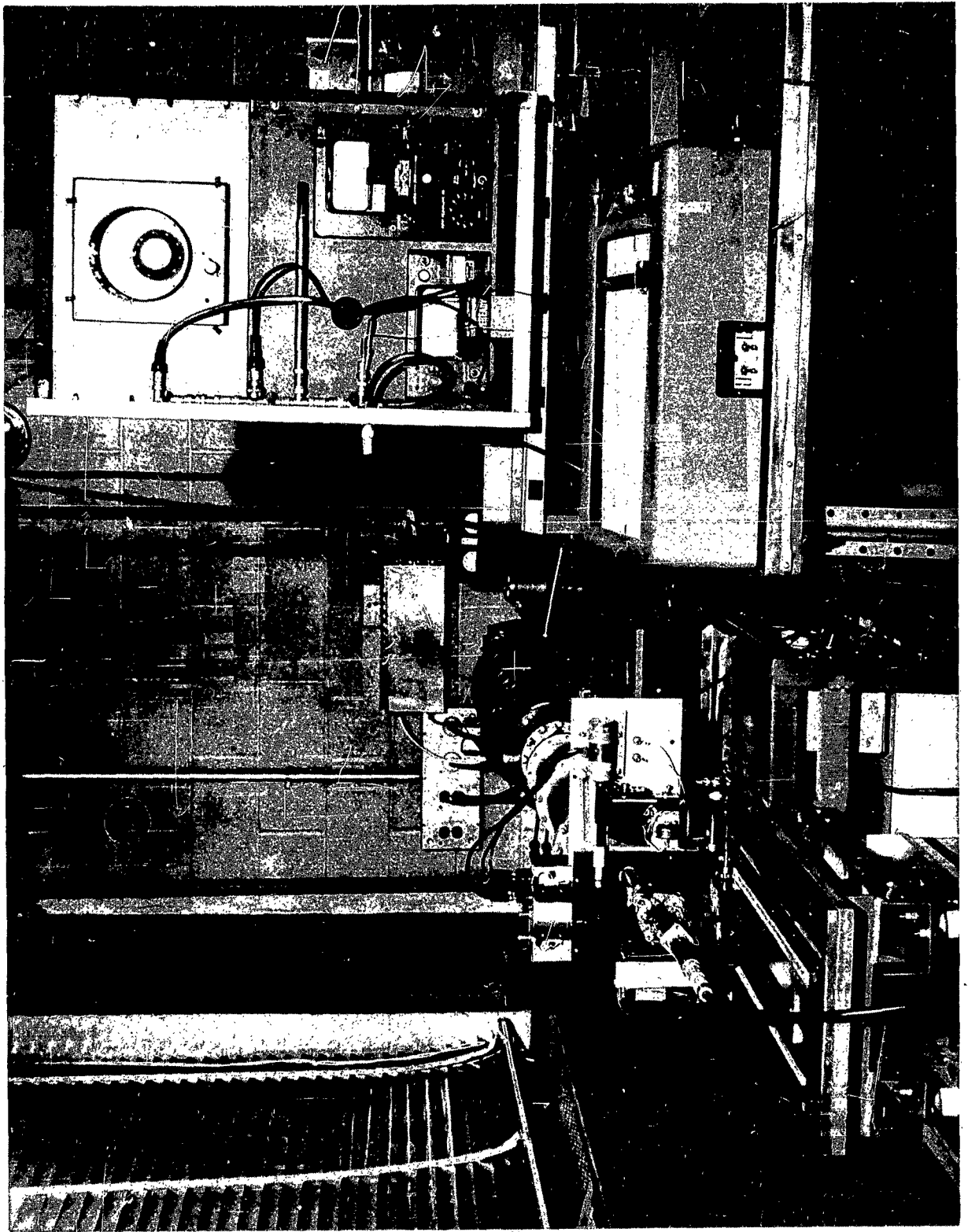
Figure 18. Beam Scanner Assembly.

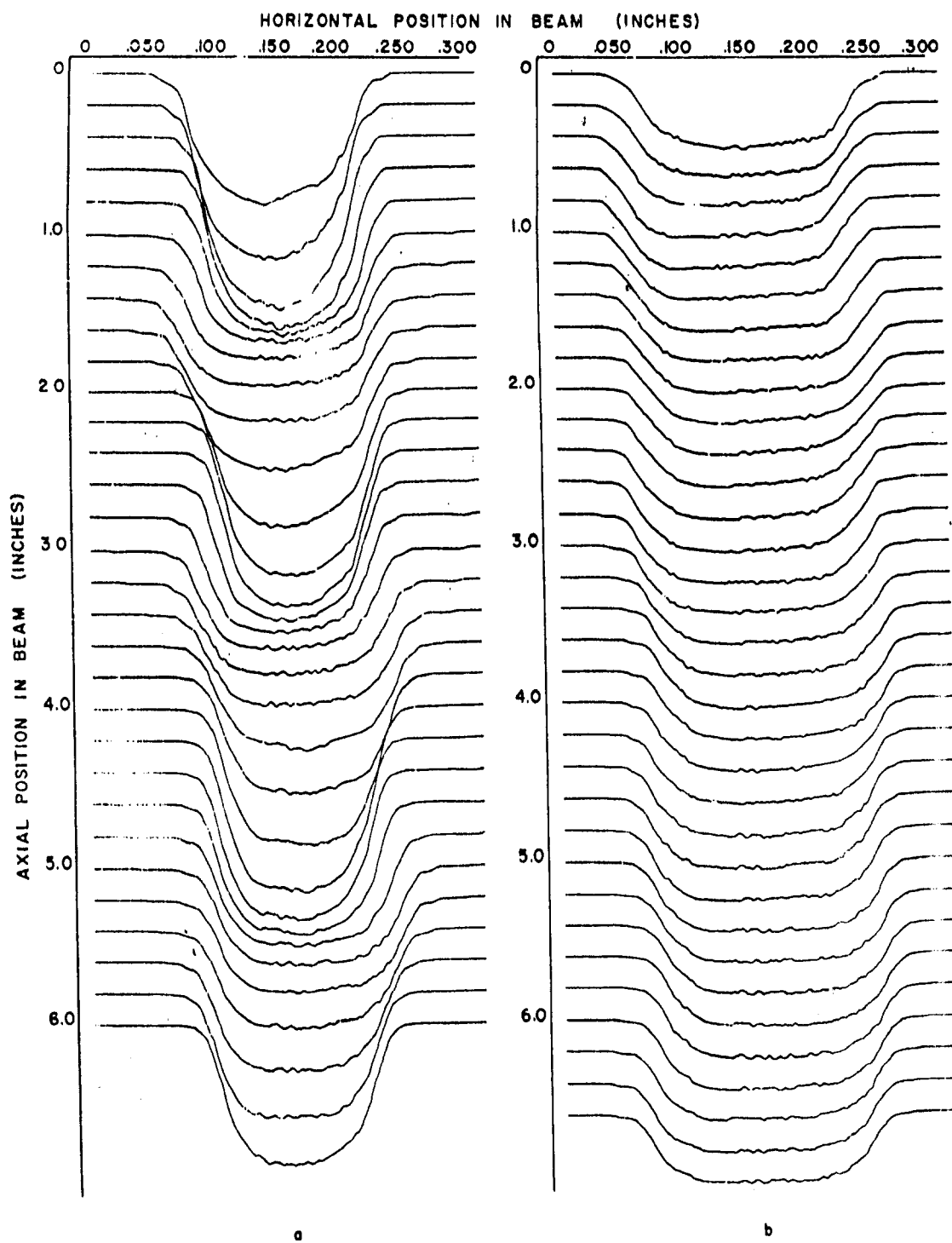Figure 19. Control Mechanism for Beam Scanner and Data-Recording System.

HORIZONTAL POSITION IN BEAM (INCHES)

Figure 20. Typical Data from which Beam Diameter Was Obtained.

It was also possible to arrange helipots to provide a voltage proportional to either the x or z position of the scanner. This made it possible to measure the beam current as a function of any one of the three positional parameters in a single scan.

APPENDIX B.   BEAM-PERTURBATION EXPERIMENT

The object of this experiment was to measure the degree of laminarity of the electron beam directly.   It was planned to identify certain electrons by placing a local perturbation on the beam, which could be tracked in the axial direction.   Because of a lack of sensitivity in the detection mechanism, it was necessary to perturb the beam so strongly to detect a change in the beam cross section that the laminar equations of motion were no longer valid.   The objectives of the experiment, therefore, were not met.   The results of the investigation are summarized here to point up the problems encountered as well as to serve as a basis for future investigations.

A.   METHODS OF PERTURBING THE BEAM

The two methods used by previous experimenters for applying a local perturbation on the beam were (1) placing an obstruction in the beam path[14, 15] and (2) removing the oxide coating from a portion of the cathode surface.[15]   These techniques were not suitable for this experiment for the following reasons:

1.   The perturbation introduced by these methods was more severe than was necessary for detection with the beam analyzer, and it was felt that a better understanding of the behavior of the unperturbed beam would be obtained if the smallest detectable perturbation were used.   Since the beam-scanning sensitivity of this analyzer was greater than that available to previous experimenters, a more refined technique was possible.

2. The d-c characteristics of the beam could not be checked. Since a rather small perturbation was anticipated, it was necessary to determine the behavior of the beam under d-c operation precisely for comparison with the perturbed behavior before the perturbation was applied. It was also important to compare the d-c behavior of the beam with the theoretical predictions before perturbing it.

Some method of perturbing the beam by an electric or magnetic field was indicated by the preceding requirements. The idea of using an electric probe was rejected. If the cathode surface is not to be disturbed, such a probe can be used only to perturb the outer edge electrons of the beam. Moreover, the addition of a mechanical structure near the beam edge in the cathode-anode region of the electron gun might disturb the focusing of the beam.

This left the magnetic field as the most promising means of perturbing the beam. Previous electron-beam studies at Cornell University had shown the possibility of using a small transverse magnetic field near the cathode to perturb the beam.[16] The field from a small perturbing coil placed just behind the cathode generated a perturbation in the beam emitted from the portion of the cathode in front of the coil. The degree of perturbation was varied by varying the current flowing through the coil. In addition, the d-c characteristics of the beam were checked simply by not passing any current through the coil. This allowed other experiments with this cathode to be made on the analyzer when data for the laminar flow study were not being taken.

B. DESIGN OF PERTURBING COIL

It was estimated that a transverse magnetic flux density of 5 gauss would be required just in front of the cathode to produce an easily detect- able perturbation. This estimate was based on a knowledge of the trans- verse field developed at peak heater current by the noninductive heater used in the STL-100 cathode and the resulting perturbation of the electron beam. As mentioned in Appendix A, this effect was not present in the d-c beam under test conditions because the cathode was pulsed at a zero of the heater current.

A plot of gauss per ampere-turn was obtained in designing the coil by assuming a single turn at the location of the perturbing coil. This plot showed that approximately 100 ampere-turns were required in the perturb- ing coil. The choice of seven turns and 15 amperes was made as the best compromise for the design criteria of size, power, and perturbing effect. Because only fringing fields of the coil were used to perturb the beam, only turns close to the cathode were effective. The use of concen- tric turns was ruled out because of the mechanical problems involved in fabricating such a coil and because this would have made the diameter of the perturbing coil too large to provide only a local perturbation. It was necessary, however, to use as many turns as possible to keep the current from being high.

The estimate of flux density per ampere developed in front of the cathode by the seven-turn coil was calculated by considering the perturbing coil to be equivalent to seven circular turns. The model used is shown in Fig- ure 21(a) and the resulting fields in Figure 21(b) . The points at which these
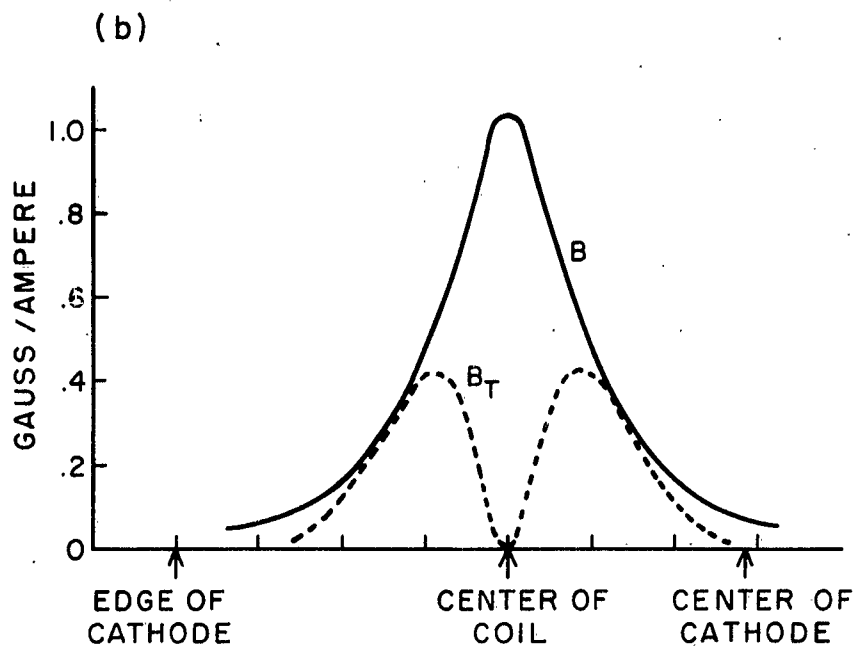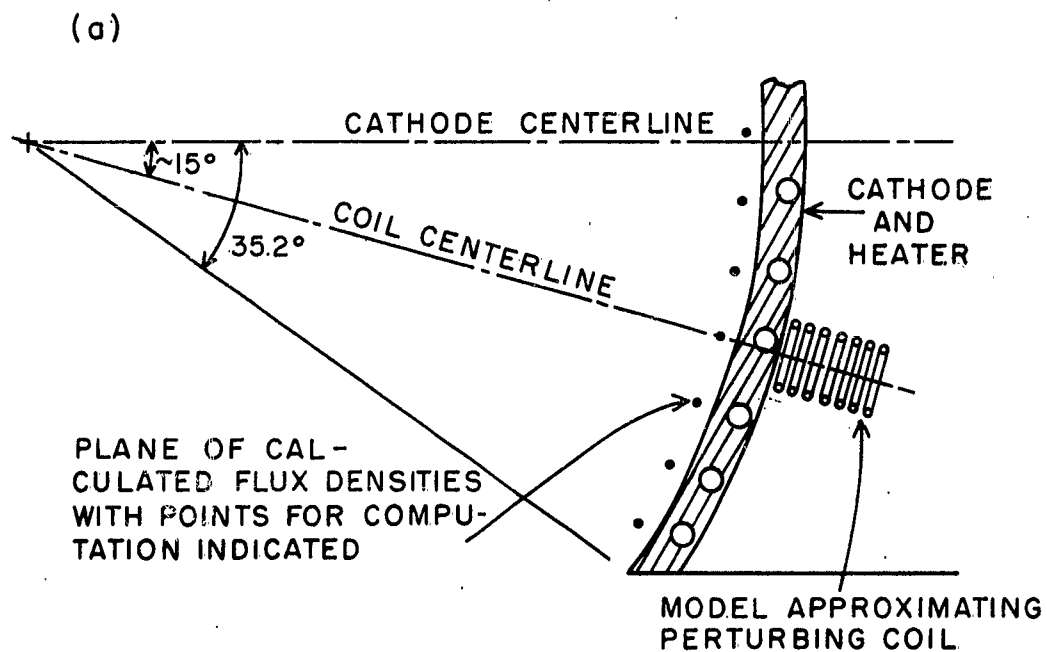
(a)

(b)

Figure 21. Calculated Flux Density Per Ampere Developed by Perturbing
Coil: (a) Schematic Showing Coil Position, (b) Field Distribution.

values were obtained were one millimeter in front of the cathode to obtain flux densities beyond the space-charge depression. This plot, using the more accurate model, shows that only 12 amperes were required in the perturbing coil to provide a sufficient transverse magnetic field, B_T.

A photograph of the coil parts and an assembled perturbing coil are shown in Figure 22. A seven-turn coil of .013-inch tungsten wire (B) was wound on the mandrel (A). The coil was then unscrewed from the mandrel, chemically cleaned, and placed on the ceramic cylinder (C), with one lead going through the center of the cylinder. Nickel straps were spot welded to the coil to hold it in place. Figure 23 is a schematic diagram showing the perturbing coil mounted behind the cathode. The heater lead support structure is omitted for simplicity. The coil was held in place by a molyb-denum spring. This permitted some freedom of movement that allowed for thermal expansions. The coil lead from the center of the ceramic cylinder was connected to the cathode, while the other lead was clamped in a block that was fastened to the focusing electrode with a ceramic insulator. The perturbing coil pulse was applied between the perturbing coil lead and the heater-cathode lead. With this arrangement the perturbing coil was always maintained at the cathode potential.

C. MOTION OF THE PERTURBED ELECTRONS

The computation of the exact trajectory of an electron moving through the magnetic field of the small coil mounted behind the cathode is a problem for a computer. In this treatment the motion will be described qualitatively.
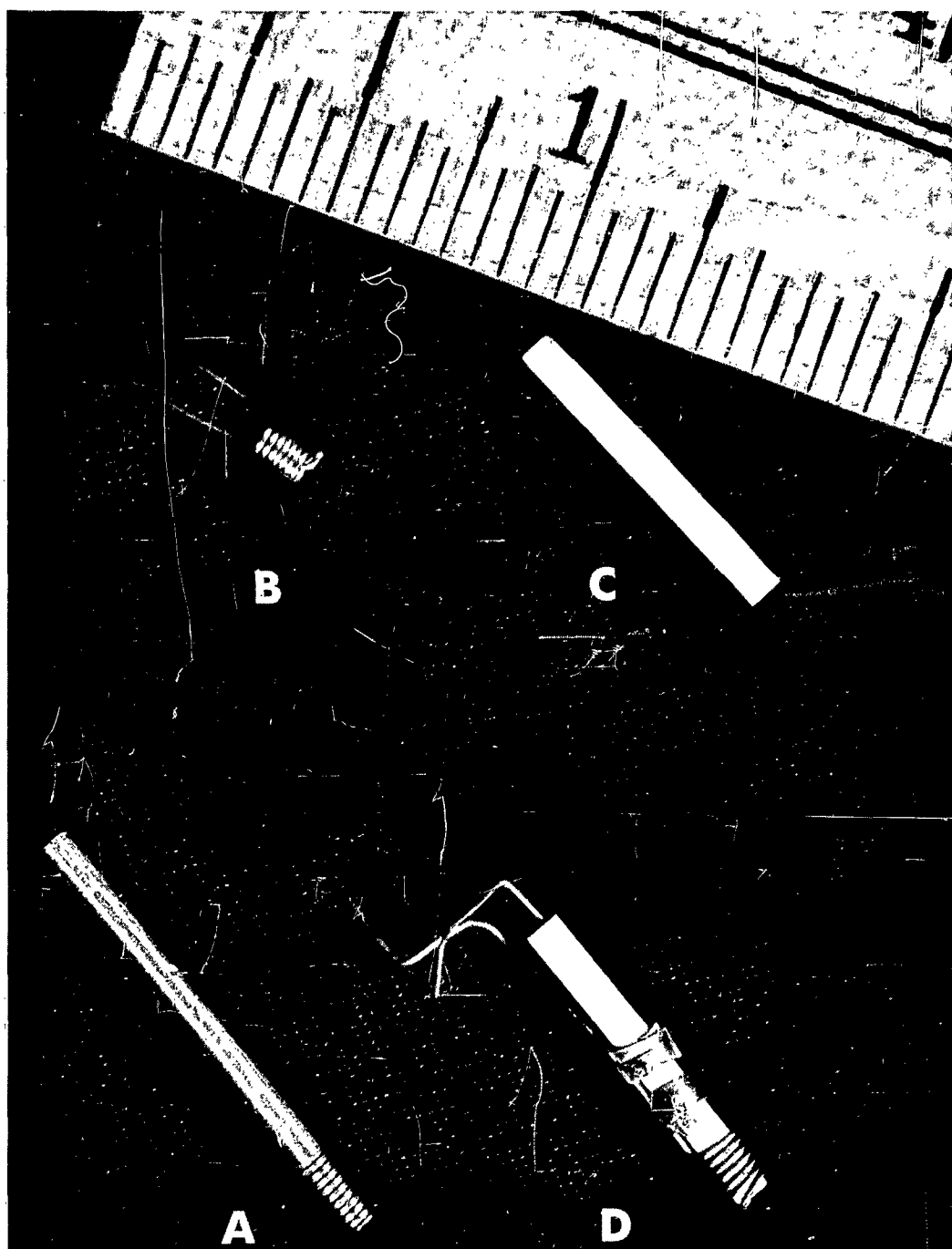
Figure 22. Perturbing Coil and Parts: (a) Mandrel for winding coil, (b) perturbing coil, (c) ceramic tubing, (d) assembled per-turbing coil.

LEAD-CLAMPING BLOCK

MOUNTING PLATE BOLTED TO FOCUS ELECTRODE

MOLYBDENUM SPRING

PERTURBING COIL LEAD TIED TO CATHODE

HEATER LEADS

REFLECTOR

CATHODE AND HEATER

PERTURBING COIL LEAD TO VACUUM SEAL
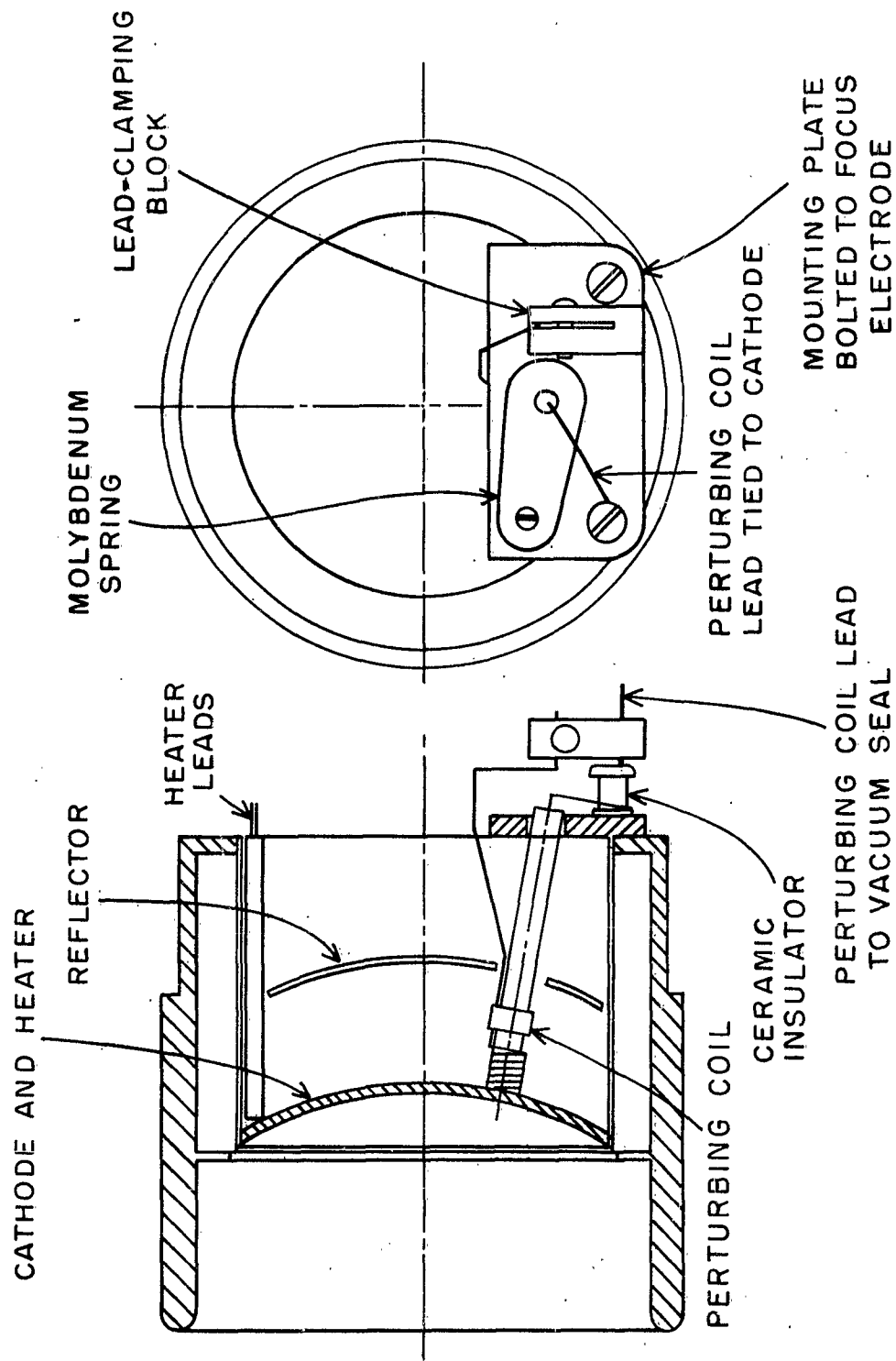
PERTURBING COIL

CERAMIC INSULATOR

Figure 23. Sketch of Perturbing Coil Mounted behind Cathode.

In the model used to describe the perturbation, the magnetic field that perturbed the electron trajectories was independent of the focusing field. Since the perturbing field strength dropped off as the inverse cube of the distance from the coil, it was assumed that this field gave certain electrons an initial translaminar velocity at the cathode and that it did not extend appreciably into the acceleration region of the gun. This assumption was supported by Figure 24, which shows the maximum value of perturbing field that occurred on the axis of the coil for a current of 15 amperes in the coil. The field strength is seen to drop off to levels which do not seriously perturb the beam beyond about .15 in. in front of the cathode. The field strength that was chosen for this level was roughly that produced by the heater at peak heater current. The countering effect of increasing
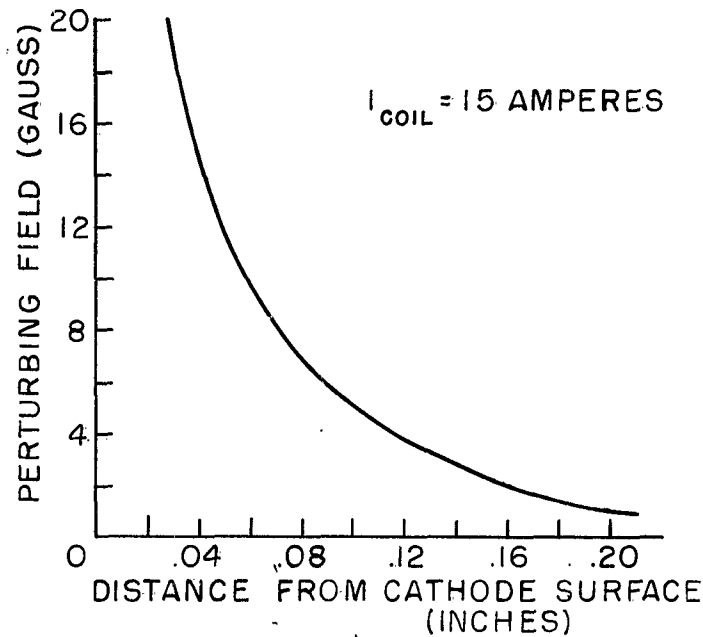

Figure 24. Maximum of Perturbing Field as Function
of Distance from Cathode.

electron velocities was not included. This led to an underestimate of the actual perturbation. The extent of the effective perturbing field in front of the cathode is shown in Figure 25.

ii. With No Focusing Field Threading the Cathode

Cutler and Hines[17] have developed a method for analyzing the effect of perturbations in Pierce-type electron guns and have applied it to determine the effects of thermal velocity in electron beams. The method assumes an ideal laminar beam, which is treated under paraxial-ray assumptions: (1) All angles of convergence and divergence of laminar flow lines are small; (2) longitudinal electric fields are uniform over a given cross section of the beam; and (3) all radial fields are proportional to the distance from the axis. One electron is perturbed at the cathode and its trajectory is traced as it moves in the laminar beam. Expressions are obtained which give, through the use of graphs, the displacement of the trajectory of this perturbed electron from the trajectory of the laminar electron that originated at the same place on the cathode. This method is readily adapted to determine the displacement of a perturbed electron from that of a laminar electron at the anode exit of the STL-100 gun where the beam is injected into the magnetic field. Figure 26 shows the geometry of the gun and some of the nomenclature required for this derivation.

The radial position of the perturbed electron is given as

$$r(z) = \mu(z) \, r_e(z) \quad , \tag{33}$$

where r_e is the radius of the edge of the beam and μ is a radial co-ordinate, which varies from zero at the beam center to unity at the beam edge. Laminar electrons follow paths of constant u.
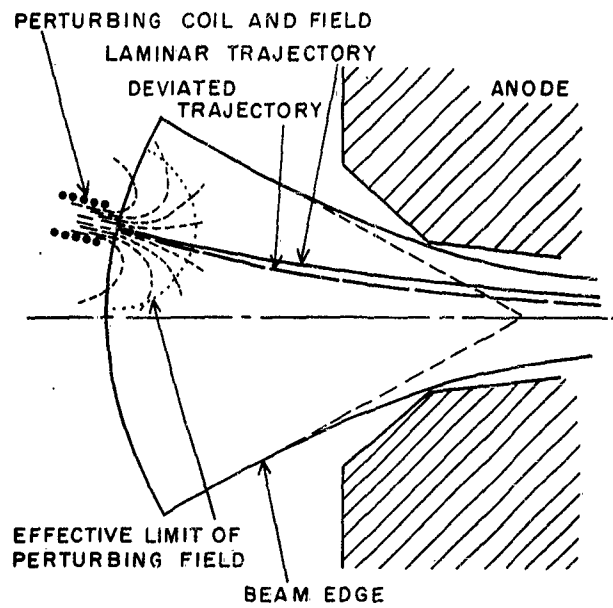
Figure 25. Extent of Effective Perturbing Field into Acceleration Region of Electron Gun.
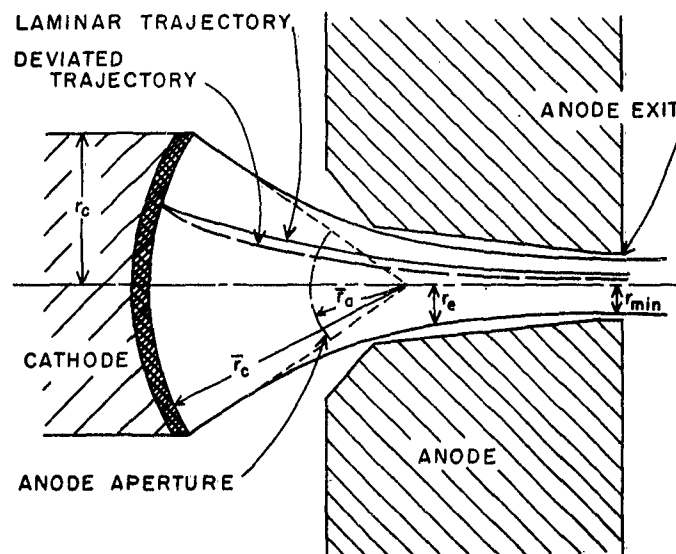

Figure 26. Diagram Showing Electron Gun Parameters Used in Tracing Perturbed Electrons.

From this Cutler and Hines[17] readily obtain

$$\mu - \mu_1 = \left(\frac{d\mu}{dt}\right)_1 \int_{t_1}^{t} \frac{dt}{\left(\frac{r_e}{r_{e_1}}\right)^2} \quad , \tag{34}$$

where the subscript 1 refers to the value at any given reference plane.
This gives the trajectory deviation Δr at any place along the axis in terms
of the perturbation velocity and position at the reference plane. From
Equation (33), this may be written as

$$\Delta r = \mu \, r_e - \mu_1 \, r_e = \left(\frac{dr}{dt}\right)_1 \frac{r_e}{r_{e_1}} \int_{t_1}^{t} \frac{dt}{\left(\frac{r_e}{r_{e_1}}\right)^2} \quad . \tag{35}$$

In the Cutler and Hines analysis, the integral on the right is sepa-
rated into two parts: the first covers the accelerating region between the
cathode and anode aperture, the second covers the drift space beyond the anode
aperture. The time $t_1 = t_{c'}$, the time at the cathode, is the lower limit.

After the appropriate substitutions and integrations, the first part
of the integral becomes:

$$\int_{t_c}^{t_a} \frac{dt}{\left(\frac{r_e}{r_c}\right)^2} = \frac{\bar{r}_c(-a_a)^{2/3}}{\sqrt{2\,\eta\,V_a}} \quad A\left(\frac{\bar{r}_c}{\bar{r}_a}\right) \quad , \tag{36}$$

where $\bar{r}_c$, and $\bar{r}_a$ are the radius of curvature of the cathode and anode aper-
ture respectively, a_a is the Langmuir parameter a evaluated at the anode,
V_a is the anode potential, and $A\left(\bar{r}_c/\bar{r}_a\right)$ is a tabulated function of $\left(\bar{r}_c/\bar{r}_a\right)$.

In the drift region beyond the anode aperture the beam diverges under the effect of the space charge in the beam. There is in addition the lens effect at the anode aperture, but this will provide only a higher-order modification to the Cutler-Hines trajectory deviation; therefore, the Cutler-Hines deviation is adequate for this application.

For the case of the shielded beam of slowly varying diameter in terms of the beam voltage and current,

$$\frac{d^2 r_e}{dt^2} = \frac{\eta}{2\pi\epsilon r_e} = \frac{\eta I_b}{2\pi\epsilon r_e \sqrt{2\eta V_a}} \quad . \tag{37}$$

When the appropriate values are substituted from the acceleration region, and several changes of variable and integration are performed, a lengthy expression for the integral on the right in Equation (35) is obtained for the beam in the drift region. This expression may be considered for the case $r_e = r_{min}$; that is, r_{min} occurs at the anode exit. That this is a valid assumption is indicated by the small amount of scalloping detected under the Brillouin focus condition described in Section III. Since the condition of zero scalloping can only be achieved if the beam is injected into the magnetic field just at $r_e = r_{min}$, the conclusion is that the beam minimum does occur at or very near the anode exit.

For the axial position at the beam minimum, the complete expression for the trajectory deviation becomes

$$\frac{\Delta r}{\left(\frac{dr}{dt}\right)_c} = \frac{\bar{r}_c}{\sqrt{2\eta V_a}} \left[\frac{r_{min}}{r_c} (-a_a)^{2/3} A\left(\frac{\bar{r}_c}{\bar{r}_a}\right) + 3\sqrt{\frac{\pi}{2}} (-a_a)^2 \, \text{erf} \sqrt{\ln} \, \frac{r_a}{r_{min}} \right] \quad . \tag{38}$$

The significant thing about this relation is that for the fixed gun design of the STL-100 and fixed beam voltage, the value of the right-hand side is a constant; thus,

$$\Delta r = \frac{K}{\mu_o} \left(\frac{dr}{dt} \right)_c . \tag{39}$$

This indicates that the trajectory deviation is directly proportional to the transverse perturbation velocity at the cathode and inversely proportional to the beam velocity. Also, though the theory was derived for the case of an initial transverse velocity in the radial direction, it may be shown to apply for off-axis electrons with initial velocities in any transverse direction. This is a consequence of the linear character of the variation of the radial fields with radius under the paraxial-ray assumption. Thus the result applies to all electrons perturbed by the magnetic field of the perturbing coil.

It should also be noted that because of the electrostatic nature of the accelerating fields, an initial transverse velocity in any given plane could be assumed to produce a trajectory deviation in that plane. This further simplifies the task of tracking electrons through the acceleration and drift regions of the gun.

The trajectory deviation of electrons entering the drift region can have both velocity and positional components. It can be expressed in terms of an $\dot{r}_c$ and a $\dot{\theta}_c$ at the cathode plane. These terms do not represent actual velocities at the cathode surface, but are mathematical equivalents which give the trajectory deviation at the anode exit.

Ideally, when the perturbed electron trajectories are extrapolated from the anode exit back to the cathode plane according to the preceding

theory, they should all intercept the cathode plane at a common point. Because the perturbing field is solenoidal, this will not occur. As a result, the "local" perturbation assumed at the cathode is, in terms of the electron motion in the beam, rather diffuse.

Some typical transverse velocities at the cathode surface are shown in Figure 27. These velocities were determined by considering the forces on an electron moving through the perturbing field. The diffuse nature of the source of the perturbations is shown. In fact, the perturbed area accounts for something approaching one-quarter of the cathode area. Because the field of the perturbing coil is confined near the coil axis and because it falls to low levels rather quickly, the diffusion is not so severe that this method of perturbing the electrons is not valid.

Now that the motion of perturbed electrons through the accelerating region of the electron gun is understood, the motion of the perturbed electrons in the beam may be described. For this treatment the laminar equa-
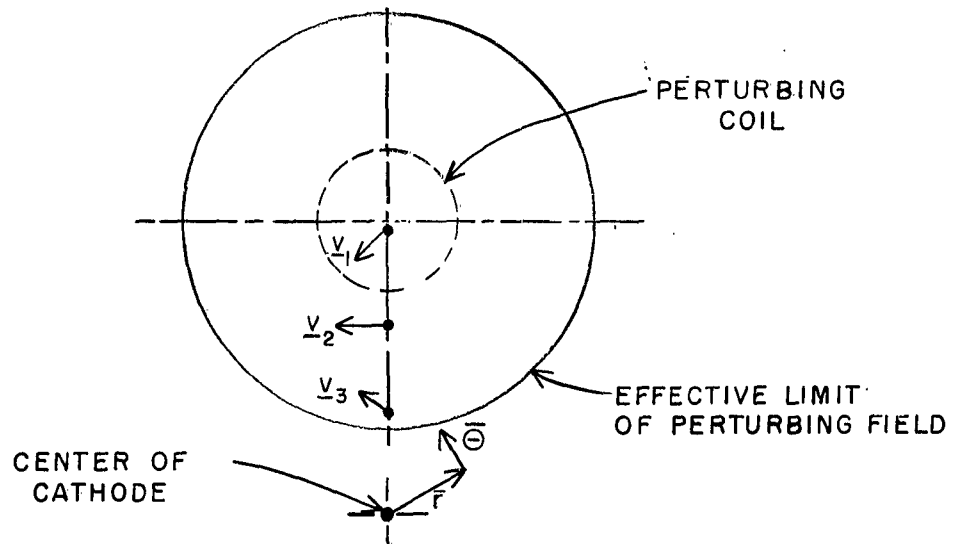
Figure 27. Typical Transverse Velocities Given to Three Electrons by the Perturbing Coil.

tion of motion previously derived will be used. This treatment is based on the so-called "translaminar theory" of a few translaminar electrons in a laminar stream used by Brewer[6] and also used in this report to explain the anomalous scallop wavelength observed by Gilmour.[3] The assumptions are (1) that the perturbed electrons do not disturb the essential laminarity of the electron beam and (2) that they remain within the beam.

The solution to Busch's theorem, Equation (8), then becomes,

$$mr^2 \dot{\theta} = er A_{\theta} - er_c A_{\theta_c} + mr_c^2 \dot{\theta}_c \quad , \tag{40}$$

or

$$\dot{\theta} = \omega_L \left(1 - \frac{g^2}{r^2}\right) + \frac{r_c^2}{r^2} \dot{\theta}_c \quad . \tag{41}$$

When the additional term, $\dfrac{r_c^2}{r^2} \dot{\theta}_c$, is carried through, the necessary algebra for the case $g = o$, Equation (16) becomes,

$$\ddot{R} + \omega_L^2 \left[R \left(1 - \frac{R_c^4}{R^4} \frac{\dot{\theta}_c^2}{\omega_L^2}\right) - \frac{1}{R} \right] = 0 \quad . \tag{42}$$

This shows that the $\dot{R}_c$ component of the perturbation does not influence the radial frequency of oscillation of the electrons. An electron with a purely $\dot{R}_c$ component at the cathode plane ($\dot{\theta}_c = 0$ for this electron) will oscillate about the laminar trajectory and remain in a constant phase relationship with it. An electron with a $\dot{\theta}_c$ component, on the other hand, will not oscillate in the radial direction with the same frequency as the laminar electron. This will give rise to a "wash-out" of the perturbation with axial position, which will become more severe as $\dot{\theta}_c$ increases.

Since the term $\dot{\theta}_c$ is squared, it might appear that the sign of this term would not affect the radial frequency of oscillation. This would be

occur only if the sign of $\dot{\theta}_c$ did not affect the axial velocity of the electron. The sign of $\dot{\theta}_c$ does affect the axial velocity,[18] however, so this effect must be considered. Since the perturbing coil used was not on the beam axis, both positive and negative signs of θ_c were given to perturbed electrons. Although detailed calculations were not made, the change in axial velocity arising from the different signs of θ_c would increase the rate of wash-out of the perturbation above that expected from Equation (42) alone.

2. With Focusing Field Threading the Cathode

Since for this study the conditions investigated were near Brillouin flow, the case of flux threading the cathode can be considered as a perturbation of the previously treated case. When $R_g \neq 0$, Equation (16) becomes:

$$\ddot{R} + \omega_L^2 \left\{ R\left[1 - \frac{R_g^4}{R^4}\left(1 - \frac{\dot{\theta}_c}{\omega_{L_c}}\right)^2\right] - \frac{1}{R}\right\} = 0 , \quad (43)$$

where $\omega_{L_c} = \dfrac{\eta B_c}{2}$.

This indicates that the presence of flux threading the cathode can affect the motion of the perturbed electrons. The sign of $\dot{\theta}_c$ alters the oscillation frequency about the laminar trajectory. Since both signs of $\dot{\theta}_c$ existed in the beam, the perturbation washed out more quickly when flux threaded the cathode. Again the velocity variation with $\dot{\theta}_c$ will exist, as when flux does not thread the cathode.

D. EXPERIMENTAL OBSERVATIONS

1. Pulse Applied to Perturbing Coil

The resistance of the coil at a cathode temperature of 825 degrees Centigrade was very nearly 1/4 ohm. The power dissipated by this coil under d-c operating conditions at a current of 12 amperes would have been too large to be practical. Since the cathode was pulsed at a .001 duty cycle, it was possible to pulse the perturbing coil in synchronism with the cathode pulse at very nearly this duty cycle. This reduced the average power dissipated by the perturbing coil to less than 3/4 watt, which was a negligible fraction of the heater power of 68 watts.

The pulse applied to the perturbing coil was synchronized with the cathode pulse, which occurred at a repetition rate of 60 cycles per second. The pulse duration of the cathode pulse was 16.7 microseconds, but a coil pulse duration of up to 100 microseconds was the design goal to allow for the use of longer pulse durations and the possibility of poor rise and fall times of the perturbing coil pulse.

A pulse transformer was used to match the extremely low impedance of the perturbing coil to a cathode follower. This transformer also provided d-c insulation between the cathode and pulsing network. A flash shield was provided to protect the primary windings from a breakdown of the insulation of the secondary windings.

A schematic of the pulsing network is shown in Figure 28. The modulator was equipped with a 60-cps sine-wave output with the phase variable with respect to a zero of the heater current. This signal was used to trigger the pulse generator in the modulator. The phase of the sine-
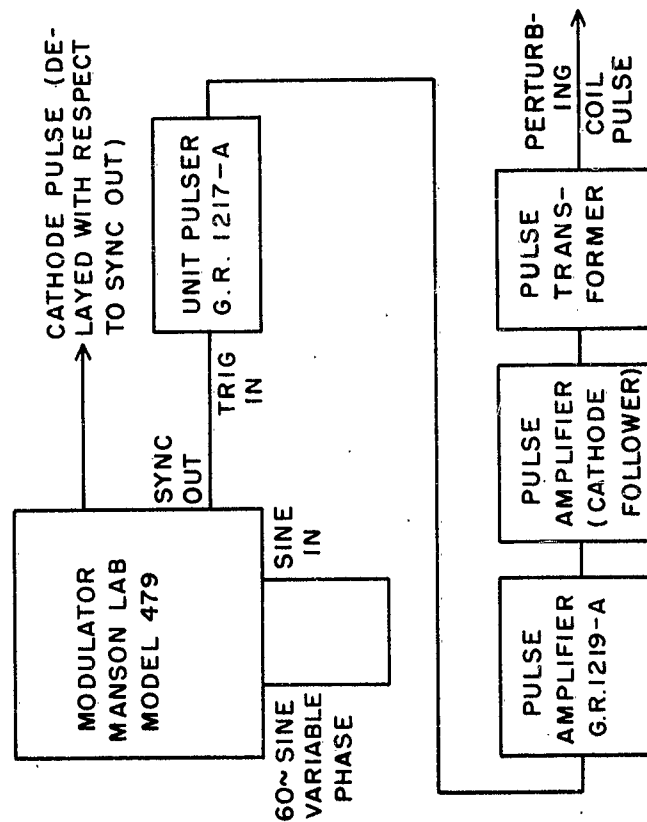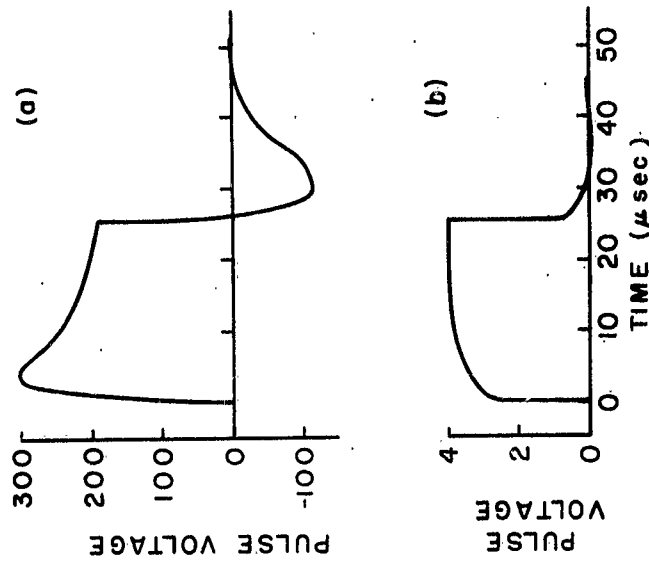
Figure 29. Perturbing Coil Pulse Wave-forms: (a) Pulse on Primary of Pulse Transformer, (b) Pulse on Secondary of Pulse Transformer.

Figure 28. Schematic of Pulsing Network.

wave trigger was adjusted to make the cathode pulse occur at a zero of the heater current. The synchronous output of the modulator was used to trigger the perturbing coil pulse. A delay line with up to 14 µsec total delay in 1.4 µsec steps was installed in the pulse generator of the modulator to allow the cathode pulse to be delayed with respect to the synchronous output. This allowed for the circuit delays in the perturbing-coil pulsing circuit and for the rise time of the perturbing-coil pulse.

A General Radio pulser and pulse amplifier were used to generate the pulse perturbing the coil. A cathode follower was needed following the General Radio pulse amplifier to provide the necessary power to the perturbing coil. This amplifier had been constructed at Cornell for another experiment. A 20-ampere pulse applied to the perturbing coil with a pulse duration of up to 100 µsec was produced. The vibration of the coil leads at the vacuum seal induced by the varying current limited the pulse current to this value for safe operation. Figure 29 shows the pulse waveforms on the primary and secondary of the pulse transformer for a 25-µsec pulse.

2. Observations on the Perturbed Beam

The perturbation was observed on the beam cross section by scanning the beam twice, once with the perturbing coil current turned on and once with the current turned off. The cross sections were superimposed on the x-y recorder so that the two results could be compared and the perturbation could be easily seen.

When the beam was pulsed, the full coil current (12 amperes) was required to obtain a measurable perturbation. This precluded varying the current to detect a possible change in the magnitude and behavior in the beam. It was originally hoped that the unperturbed beam could be evaluated

by extrapolating to zero the results obtained by perturbing the beam at several values of coil current.

The behavior of the perturbed beam was as expected. The perturbation was observed over a distance of six to eight inches from the anode exit. In this region it seemed to rotate about the axis at roughly the Larmor angular velocity. Beyond this point the perturbation washed out. This behavior would be expected from the previous theoretical discussion. At a distance of 16-18 inches from the anode exit two perturbations appeared on the beam on opposite sides of the beam center. (That two localized perturbations were seen was a little surprising and has not been explained.)

The coil was modulated with a 500 kc/s r-f signal detected with a receiver in order to increase the sensitivity of the measurements. The higher harmonics of the beam pulse made detection of the perturbation impossible with this technique.

E. RECOMMENDATIONS FOR FUTURE STUDY

This method of probing the beam has shown some promise. In order to obtain useful results, however, some improvements in the detection sensitivity must be made.

1. Perturb alternate pulses of the beam. This would put a 30-cycle perturbation on the beam. A low-pass filter in series with the detected beam current will allow the 60-cycle beam-pulse component to be eliminated. This 30-cycle perturbation could be amplified and visually displayed on an oscilloscope to obtain much greater sensitivity than the method described in Section D. A circuit for perturbing alternate pulses of the electron beam has been built and a schematic of it is shown in Figure 30.

-73-

2. __Use a smaller pin-hole.__ If a .002 in. or .003 in. pinhole is used instead of the .005-inch pinhole used in taking data thus far, the amount of trajectory deviation required would be much less. This should allow the maximum benefit to be obtained from the increase in sensitivity described above.

3. __Investigate the first few inches of beam after the anode exit.__ Since the perturbation blurs beyond 8-10 inches from the anode exit, the increase in sensitivity and resolution resulting from using a smaller pin-hole and perturbing alternate pulses of the beam would be of little value unless measurements were taken close to the anode exit.
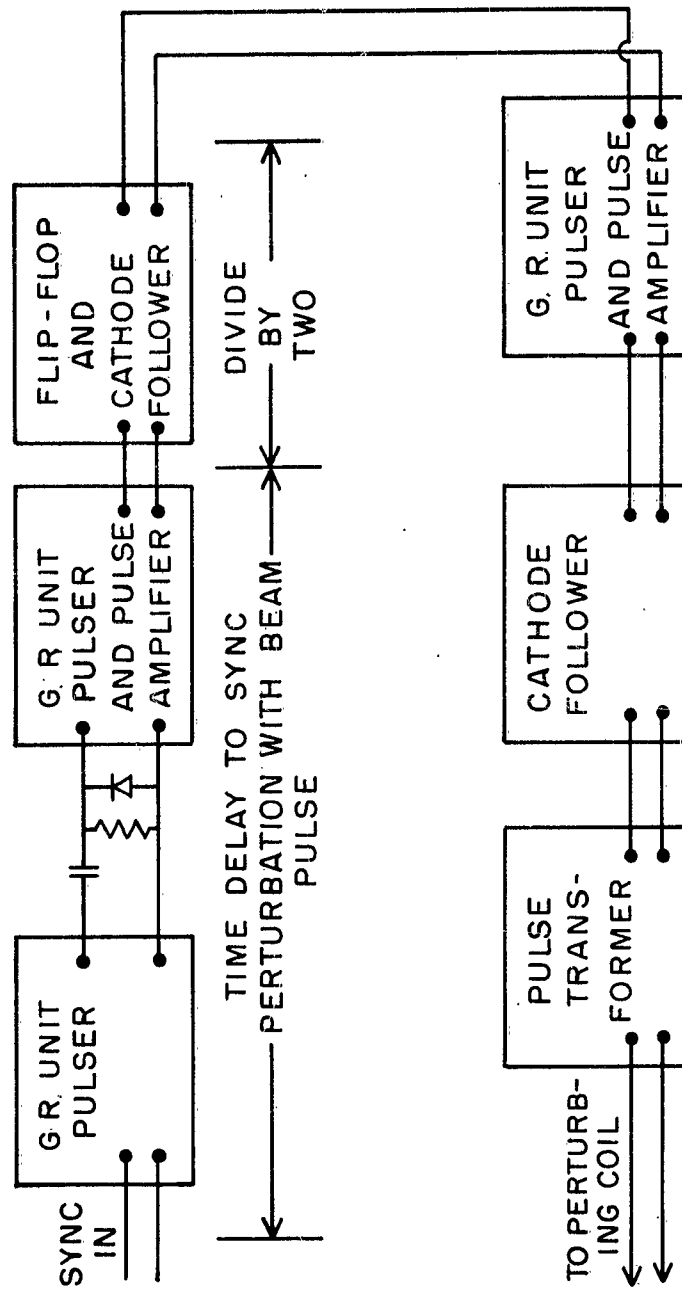
Figure 30. Circuit for Perturbing Alternate Beam Pulses.

REFERENCES

1. A. S. Gilmour, Jr., "The Velocity Distribution in a Velocity-modulated Electron Beam from a Shielded Pierce Gun, " Research Report EE 507, Cornell University, August 1961.

2. L. Brillouin, "A Theorem of Larmor and its Importance for Electrons in a Magnetic Field, "Phys. Rev., 66, (1945), pp. 260-266.

3. A. S. Gilmour, Jr., "A Beam Tester for Studying the Characteristics of Velocity-modulated Electron Beams, " Research Report EE 495, Cornell University, May 1961.

4. C. C. Wang, "Electron Beams in Axially Symmetric Electric and Magnetic Fields, " Proc. I.R.E., 38 (February 1950), pp. 135-147.

5. J. R. Pierce, Theory and Design of Electron Beams, New York: D. Van Ostrand, (1949), p. 153.

6. G. R. Brewer, "Some Characteristics of a Magnetically Focused Electron Beam, " J. App. Phys., 30 (July 1959), pp. 1022-1038.

7. J. L. Palmer and C. Süsskind, "Effects of Transverse Velocities in Magnetically Focused Cylindrical Electron Beams, " in Proc. Int. Conf. on Microwave Tubes, Munich, (June 7 to 11, 1960), New York: Academic Press, (1961), pp. 456-460.

8. R. D. Frost, O. T. Purl, and H. R. Johnson, "Electron Guns for Forming Solid Beams of High Perveance and High Convergence, " Proc. I.R.E., 50 (August 1962), pp. 1800-1807.

9. W. W. Rigrod, "Noise Spectrum of Electron Beam in Longitudinal Magnetic Field," 'Bell Sys. Tel. Jour., 36 (July 1957), pp. 831-889.

10. T. G. Mihran, "Scalloped Beam Amplification," Trans. I.R.E., ED-3 (January 1956), p. 32.

11. J. R. Pierce and L. R. Walker, "Brillouin Flow with Thermal Velocities," J. App. Phys., 24 (October 1953), p. 1328.

12. C. C. Cutler and J. A. Saloom, "Pin-Hole Camera Investigation of Electron Beams," Proc. I.R.E., 43 (March 1955), pp. 299-306.

13. G. F. Herrman, "Optical Theory of Thermal Velocity Effects in Cylindrical Electron Beams," J. App. Phys., 29 (February 1958) pp. 127-136.

14. H. F. Webster, "Structure in Magnetically Confined Electron Beams," J. App. Phys., 28 (December 1957), pp. 1388-1397.

15. A. Askin, "Electron Beam Analyzer," J. App. Phys., 28 (May 1957), pp. 564-569.

16. A. S. Gilmour, Jr., Private Communication.

17. C. C. Cutler and M. E. Hines, "Thermal Velocity Effects in Electron Guns," Proc. I.R.E., 43 (March 1955), pp. 307-315.

18. J. L. Palmer, "Laminar Flow in Magnetically Focused Electron Beams," Trans. I.R.E., ED-6 (July 1959), pp. 262-269.